Cyclophilin A knock-out mice develop a pure frontotemporal dementia phenotype with marked TDP-43 pathology

Pasetto L.[1], Pozzi S.[2], Micotti E.[3], Cerovic M.[3], Carli M.[3], Forloni G.[3], Bonetto V.[1*]

[1]Department of Biochemistry and Molecular Pharmacology, Istituto di Ricerche Farmacologiche Mario Negri IRCCS, 20156 Milano, Italy

[2]CERVO Brain Research Centre, Quebec city, Québec, Canada

[3]Department of Neuroscience, Istituto di Ricerche Farmacologiche Mario Negri IRCCS, 20156 Milano, Italy

[*]Correspondence: Valentina Bonetto, Department of Biochemistry and Molecular Pharmacology, Istituto di Ricerche Farmacologiche Mario Negri IRCCS, Via Mario Negri 2, 20156 Milano, Italy; Email: valentina.bonetto@marionegri.it

Running Head: PPIA-/- mice display an FTD-like phenotype

ABSTRACT

Frontotemporal dementia (FTD) is a common cause of early-onset dementia, characterized by frontotemporal lobar degeneration and considerable clinical, genetic and neuropathological heterogeneity. Several mouse models of FTD have been generated targeting genes with known pathogenic roles. However, each of these models recapitulates only certain aspects of the human disease. Cyclophilin A (PPIA) is a multifunctional protein abundantly expressed in the brain, with double-edged functions. Intracellularly, it is mainly protective as a foldase and molecular chaperone with scaffolding properties. Extracellularly, it behaves as a proinflammatory cytokine able to activate an aberrant inflammatory response. In a previous work, we found that PPIA governs TDP-43 functions and its deficiency exacerbates disease in a mouse model of ALS. Selective inhibition of extracellular PPIA rescued motor neurons and increased survival. To decipher PPIA's functions in the central nervous system, we planned a deep neuropathological and behavioral characterization of *PPIA* knock-out (*PPIA-/-*) mice throughout their lifespan. They develop a neurodegenerative disease that recapitulates key features of the behavioral variant of FTD associated with TDP-43 pathology. *PPIA-/-* mice present progressive hippocampal and cortex atrophy, with neuronal death and clear-cut TDP-43 pathology that include fragmentation, hyperphosphorylation, and cytoplasmic mislocalization/nuclear clearing. Mice exhibit increased disinhibition, defects in social behavior, but no memory and motor impairment. On a molecular level, our findings indicate that PPIA is involved in multiple genes and pathways that have a dominant protective effect in the brain, and is fundamental for TDP-43 function. Considering that an impaired interaction of TDP-43 with PPIA has been observed in ALS/FTD patients, the *PPIA-/-* mouse is a useful experimental model to investigate the mechanism at the basis of TDP-43 pathology and develop novel therapeutic approaches for ALS/FTD and possibly other TDP-43 proteinopathies.

Keyword: TDP-43 pathology, mouse model, RNP complex, GRN

INTRODUCTION

Frontotemporal dementia (FTD) is a common cause of early-onset dementia. The prevalence is 10.8 per 100,000 individuals with about 30% of patients having a strong family history (Coyle-Gilchrist et al., 2016; Wood et al., 2013). FTD is characterized by frontotemporal lobar degeneration (FTLD) and comprises a spectrum of neurodegenerative disorders with considerable clinical, genetic and neuropathological heterogeneity (Olney et al., 2017). Clinically FTD may involve frontal and/or anterior temporal lobes, insular cortex, and subcortical structures, resulting in two main phenotypes, primary progressive aphasia and the behavioral variant (bvFTD), which is the most prevalent and involves cognitive decline and behavioral dysfunctions (Rascovsky et al., 2011).

Genetically, mutations in *C9orf72*, *GRN* and *MAPT* are the most frequent and are found in the sporadic and familial forms (Ferrari et al., 2019). Neuropathologically, 45% of FTD patients present tau inclusions (FTLD-Tau), together with *MAPT* mutations; 50% have TDP-43 pathology (FTLD-TDP), with *GRN*, *C9orf72*, *TARDBP*, *VCP* and other rare gene mutations, and the remaining cases have FUS inclusions and *TAF15* and *EWS* co-aggregated (FTLD-FET) (Irwin et al., 2015; Neumann and Mackenzie, 2019). Finally, there is a significant genetic and neuropathological overlap between FTD and amyotrophic lateral sclerosis (ALS) with up to 40% of FTD patients developing motor dysfunction (Burrell et al., 2011).

This extreme complexity makes modeling the disease in mice to decipher pathogenesis and develop effective therapies difficult. Several mouse models of FTD have been generated, targeting genes with known pathogenic roles. However, each model recapitulates only certain aspects of the human disease (Tan et al., 2017).For instance, TDP-43 pathology in mice is absent or mild, is not always linkedto neurodegeneration and behavioral phenotypes, and may show a mixed phenotype that includes motor impairment.

Cyclophilin A (PPIA), also known as peptidyl-prolyl cis-trans isomerase A, is a member of the immunophilin family, widely distributed in all tissues, particularly the brain, where it localizes mainly in neurons (Göldner and Patrick, 1996; Ryffel et al., 1991). Despite its abundance, its primary function in the brain remains largely undefined. PPIA was initially discovered as the host cell receptor of the immunosuppressive drug cyclosporin A (Handschumacher et al., 1984). Later PPIA was recognized as an enzyme with peptidyl-prolyl *cis-trans* isomerase (PPIase) activity (Fischer et al., 1989), essential to protein

folding *in vivo*. PPIA is involved in several cellular processes, intra- and extracellularly. Inside the cells, besides promoting *de novo* protein folding, PPIA acts as a molecular chaperone and protects against stress conditions such as oxidative stress and protein misfolding (Boulos et al., 2007; Choi et al., 2007; Lauranzano et al., 2015; Lee et al., 1999).

Immunophilins exert their diverse cellular functions often in hetero-oligomeric complexes, probably regulating the architecture, assembly and disassembly of the complexes by their scaffolding properties (Rein, 2020). PPIA interacts with several heterogeneous nuclear ribonucleoproteins (hnRNPs), including TDP-43, and plays a role in the stability of the RNP complexes, suggesting an involvement in RNA metabolism (Lauranzano et al., 2015). A number of reports suggest that PPIA also regulates protein trafficking and subcellular localization. For example, it is necessary for CXCR4-mediated nuclear export of hnRNP A2 and for nuclear translocation of the apoptosis-inducing factor (AIF) (Cande et al., 2004; Pan et al., 2008).

Extracellularly, PPIA behaves as a pro-inflammatory cytokine (Sherry et al., 1992). It is secreted by different cell types, including neurons and glial cells, in response to stress, promoting neuroinflammation and motor neuron death (Hoffmann and Schiene-Fischer, 2014; Pasetto et al., 2017).

Although PPIA has been involved in several human diseases, some neurodegenerative, its role in pathogenesis has not been established (Nigro et al., 2013). We firstly reported that PPIA is altered in amyotrophic lateral sclerosis (ALS) animal models and patients (Basso et al., 2009; Massignan et al., 2007; Nardo et al., 2011). Next, we demonstrated that low levels of PPIA in peripheral blood mononuclear cells (PBMCs) of ALS patients are associated with an early onset of the disease (Filareti et al., 2017) and a short disease duration (Luotti et al., 2020). In agreement with this, PPIA deficiency exacerbated aggregation and accelerated disease progression in a $SOD1^{G93A}$ mouse model of ALS (Lauranzano et al., 2015). Finally, we found that PPIA governs key TDP-43 functions, probably by influencing its folding and localization. In fact PPIA deficiency induced TDP-43 mislocalization and aggregation, and affected the expression of a number of TDP-43 target genes.

In previous work, we observed that *PPIA* knock-out (*PPIA*-/-) mice presented features of TDP-43 pathology but without any overt clinical phenotype up to four months of age. Here, we have characterized *PPIA*-/- mice neuropathologically and behaviorally throughout their entire lifespan and found that with aging they develop an FTD phenotype associated with behavioral deficits and TDP-43 pathology, resembling

closely the human disease and providing new insights into the pathogenic mechanisms involved in TDP-43 proteinopathies.

MATERIALS AND METHODS

Animal model

Procedures involving animals and their care were conducted in conformity with the following laws, regulations, and policies governing the care and use of laboratory animals: Italian Governing Law (D.lgs 26/2014; Authorization 19/2008-A issued March 6, 2008 by Ministry of Health); Mario Negri Institutional Regulations and Policies providing internal authorization for persons conducting animal experiments (Quality Management System Certificate, UNIENISO9001:2008, Reg.No.6121); the National Institutes of Health's Guide for the Care and Use of Laboratory Animals (2011 edition), and European Union directives and guidelines (EEC Council Directive, 2010/63/UE). The Mario Negri Institutional Animal Care and Use Committee and the Italian Ministry of Health (Direzione Generale della Sanità Animale e dei Farmaci Veterinari, Ufficio 6) prospectively reviewed and approved the animal research protocols of this study (prot. no. 14-02/C and 9F5F5.60) and ensured compliance with international and local animal welfare standards.

Animals were bred and maintained at the Istituto di Ricerche Farmacologiche Mario Negri-IRCCS, Milan, Italy, under standard conditions: temperature 21 ± 1°C, relative humidity 55 ± 10%, 12h light schedule, and food and water ad libitum. Before every analysis, animals were deeply anesthetized with ketamine hydrochloride (IMALGENE, 100 mg/kg; Alcyon Italia) and medetomidine hydrochloride (DOMITOR, 1 mg/kg; Alcyon Italia) by intraperitoneal injection and killed by decapitation.

We obtained *PPIA*-/- mice (strain 129S6/SvEvTac Ppiatm1Lubn/Ppiatm1Lbn; stock no. 005320) from The Jackson Laboratory; they were maintained on a 129S6/SvEvTac background. *PPIA* -/- mice were originally generated and characterized as previously described (Colgan et al., 2000; Colgan et al., 2004). The 129S6/Sv genetic background was used for biochemistry, immunohistochemistry, long-term potentiation and magnetic resonance analysis. *PPIA*-/- mice on C57BL/6J genetic background, kindly provided by Dr. Bradford C. Berk (University of Rochester Medical Center, Rochester, New York, USA), were used for behavioral tests and biochemical experiments. Genotyping for *PPIA* was done by standard PCR on DNA tail biopsies, using primer sets designed by The Jackson Laboratory.

Subcellular fractionation

Nuclear and cytoplasmic fractions were separated from mouse cortex and cerebellum as described (Lauranzano et al., 2015; Pasetto et al., 2017). Briefly, tissues were homogenized in six volumes (w/v) of buffer A (10 mM Tris-HCl pH 7.4, 5 mM MgCl2, 25 mM KCl, 0.25 M sucrose, 0.5 mM DTT) containing a protease inhibitors cocktail (Roche), and centrifuged at 800 xg for 10 min at 4°C. The supernatant was centrifuged twice at 800 xg for 10 min at 4°C (cytoplasmic fraction). The pellet was resuspended in three volumes of buffer A and centrifuged three times at 800 xg for 10 min at 4°C. The pellet was resuspended in one volume of buffer A and one volume of buffer B (10 mM Tris-HCl pH 7.4, 5 mM MgCl2, 25 mM KCl, 2 M sucrose) containing a protease inhibitors cocktail, and loaded on a layer of one volume of buffer B. Samples were ultracentrifuged at 100,000 xg for 45 min at 4°C. The pellet (nuclear fraction) was resuspended in 100 µl of buffer A, centrifuged at 800 xg for 10 min at 4°C and resuspended in 40 µL buffer A.

Extraction of detergent-insoluble and soluble proteins

Mouse tissues were homogenized in 10 volumes (w/v) of buffer, 15 mM Tris-HCl pH 7.6, 1 mM DTT, 0.25 M sucrose, 1 mM $MgCl_2$, 2.5 mM EDTA, 1 mM EGTA, 0.25 M sodium orthovanadate, 2 mM sodium pyrophosphate, 25 mM NaF, 5 µM MG132, and a protease inhibitors cocktail (Roche), essentially as described (Lauranzano et al., 2015). Samples were centrifuged at 10,000 xg at 4°C for 15 min and supernatant 1 was collected in a new tube. The pellet was suspended in ice-cold homogenization buffer with 2% of Triton X100 and 150 mM KCl, sonicated and shaken for 1h at 4°C. The samples were then centrifuged twice at 10,000 xg at 4°C for 10 min to obtain the Triton-insoluble fraction (TIF) pellet and supernatant 2. Supernatants 1 and 2 were pooled, as the Triton-soluble fraction. Immunoreactivity was normalized to protein loading (Ponceau red staining). The amount of Triton-resistant proteins isolated from the tissue was normalized to the soluble protein extracted. Proteins were quantified by the BCA protein assay (Pierce).

Immunoblotting

Protein levels were determined using the BCA protein assay (Pierce). For western blot (WB), samples (15 µg) were separated in 12% SDS-polyacrylamide gels and transferred to polyvinylidene difluoride membranes (Millipore), as described previously (Lauranzano et al., 2015). For dot blot, proteins (3 µg) were loaded directly onto nitrocellulose Trans-blot transfer membranes (0.45 µm; Bio-Rad),depositing each sample on the membrane by vacuum filtration, as described previously (Basso et al., 2009; Filareti et al., 2017; Massignan et al., 2007; Nardo et al., 2011; Pasetto et al., 2017). WB and dot blot membranes were blocked with 3% (w/v) BSA (Sigma-Aldrich) and 0.1% (v/v) Tween 20 in Tris-buffered saline, pH 7.5, and incubated with primary antibodies according to the manufacturer's protocol and then with peroxidase-conjugated secondary antibodies (GE Healthcare). Antibodies used for immunoblot are the following: rabbit polyclonal anti-human TDP-43 antibody (1:2500, Proteintech; RRID: AB_2200505); mouse monoclonal anti-human phospho Ser409/410 TDP-43 (phTDP-43) antibody (1:2000, Cosmo Bio Co., LTD; RRID: AB_1961900); rabbit polyclonal anti-ubiquitin (1:800, DAKO; RRID: AB_2315524); mouse monoclonal anti-hnRNPA2/B1 (1:2000, Abnova; RRID: AB_425488); rabbit polyclonal anti-human SOD1 antibody (1:1000, Millipore; RRID: AB_2704226); mouse monoclonal FUS/TLS antibody (1:200, Santa Cruz; RRID: AB_2105208); mouse monoclonal anti-PSD95 antibody (1:10000, Neuromab; RRID: AB_2292909); rabbit polyclonal anti- synaptophysin antibody (1:5000, Synaptic System; RRID: AB_887905); rabbit polyclonal anti-human progranulin (1:250; Invitrogen; RRID: AB_2533461); rabbit polyclonal anti-TIA1 antibody (1:1000, Proteintech; RRID: AB_2201427); mouse monoclonal anti-GFAP antibody (1:1000; Millipore; RRID:AB_94844); rabbit polyclonal anti-Iba1 (1:500; Wako; RRID:AB_839504) goat anti-mouse or anti-rabbit peroxidase-conjugated secondary antibodies (respectively 1:20000 and 1:10000, GE Healthcare). Blots were developed with the Luminata Forte Western Chemiluminescent HRP Substrate (Millipore) on the ChemiDoc™ Imaging System (Bio-Rad). Densitometry was done with Progenesis PG240 version 2006 software (Nonlinear Dynamics). The immune reactivity of the different proteins was normalized to Ponceau Red staining (Fluka).

Immunohistochemistry

Mice were anesthetized and perfused transcardially with 50 mL of PBS followed by 100 mL of 4% paraformaldehyde (Sigma-Aldrich) solution in PBS. Brain and spinal cord were rapidly removed, postfixed

for 3h, transferred to 20% sucrose in PBS overnight and then to 30% sucrose solution until they sank, frozen in N-pentane at 45°C and stored at ± 80°C. Before freezing, spinal cord was divided into cervical, thoracic, and lumbar segments and included in Tissue-tec OCT compound (Sakura).

Coronal sections (30 µm; four slices per mouse) of brain were then sliced and immunohistochemistry for TDP-43 (Proteintech), pTDP-43 (Cosmo Bio Co., LTD), GFAP (Millipore) and Iba1 (DBA) was done. Briefly, slices were incubated for 1h at room temperature with blocking solutions (TDP-43 and pTDP-43: 0.2% Triton X100 plus 2% NGS; GFAP: 0.4% Triton X100 plus 3% NGS; Iba1: 0.3% Triton X100 plus 10% NGS),then overnight at 4°C with the primary antibodies (TDP-43, 1:200; pTDP-43, 1:1000; GFAP, 1:2500; Iba1, 1:1000). After incubation with biotinylated secondary antibody (1:200; 1h at room temperature; Vector Laboratories) immunostaining was developed using the avidin–biotin kit (Vector Laboratories) and diaminobenzidine (Sigma). Coronal brain sections (30 µm; four slices per mouse) and lumbar spinal cord (30 µm; twelve slices per mouse) were stained with 0.5% cresyl violet to detect the Nissl substance of neuronal cells. GFAP-, Iba1- and Nissl-stained sections were collected at 20 X with an Olympus BX-61 Virtual Stage microscope so as to have complete stitching of the whole section, with a pixel size of 0.346 µm. Acquisition was done over 6-µm-thick stacks with a step size of 2 µm. The different focal planes were merged into a single stack by mean intensity projection to ensure consistent focus throughout the sample. Finally, signals were analyzed for each slice with ImageJ software.

Magnetic resonance imaging analysis

Magnetic resonance imaging (MRI) analysis was done in six- and twelve-month-old mice, as previously described (Mancini et al., 2017). Briefly animals were anesthetized with isoflurane in a mixture of O_2 (30%) and N_2O (70%). Body temperature was maintained at ~37°C by a warm water circulated heating cradle. Imaging was done on a 7 T small bore animal Scanner (Bruker Biospec, Ettlingen, Germany). A 3D RARE T2 weighted sequence was used to assess anatomical changes. The volume measurements of structural MRI images were obtained using Java-based custom-made software. ROIs were selected manually and drawn on the images for volumetric assessment. Whole brain, hippocampus, cortex, frontal cortex and cerebellum were measured. Frontal cortex was quantified separately from the rest of the cortex, from bregma 3.20 mm to

bregma 1.54 mm. Data from each animal were obtained by integration of the averaged ROI area for slice thickness and normalized to whole brain volume.

Long-term potentiation analysis

For extracellular recordings coronal brain slices (350 µm) were cut in ice-cold modified artificial cerebrospinal fluid (aCSF) containing the following: 87 mM NaCl, 2.5 mM KCl, 1 mM NaH_2PO_4, 75 mM sucrose, 7 mM $MgCl_2$, 24 mM $NaHCO_3$, 11 mM D-glucose, and 0.5 mM $CaCl_2$. Slices where then transferred to an incubating chamber, submerged in aCSF containing: 130 mM NaCl, 3.5 mM KCl, 1.2 mM NaH_2PO_4, 1.3 mM $MgCl_2$, 25 mM $NaHCO_3$, 11 mM D-glucose, 2 mM $CaCl_2$, constantly bubbled with 95% O_2 and 5% CO_2 at room temperature. Slices were incubated in this condition for at least 1h before recording, then transferred into a submerged recording chamber and perfused with oxygenated aCSF at a rate of 2 mL/min at a constant temperature of 28-30ºC.

Field EPSPs (fEPSPs) were recorded with glass micropipettes filled with 3 M NaCl electrode in CA1 stratum radiatum. The Schaffer collaterals were stimulated with a bipolar twisted Ni/Cr stimulating electrode. Stimuli were delivered by a Constant Voltage Isolated Stimulator (Digitimer Ltd., Welwyn Garden City, UK). Data were amplified and filtered (10Hz to 3kHz) by a DAM 80 AC Differential Amplifier (World Precision Instruments, Sarasota, FL), and digitized at 10 kHz by a Digidata 1322 (Molecular Devices, Foster City, CA). Long-term potentiation (LTP) was induced by a 4-theta-burst tetanus stimulation protocol (each burst consists of four pulses at 100 Hz with 200 ms inter-burst intervals). LTP recordings in which the amplitude of the presynaptic fiber volley changed by more than 20% were discarded.

Micro-CT

Micro-CT was done with an Explore Locus micro-CT scanner (GE Healthcare) without contrast agents. Before the analysis, mice were anesthetized with a continuous flow of 3% isofluorane/oxygen mixture and placed prone on the micro-CT bed. A micro-CT lower resolution (Bin-4) protocol was employed using 80 kV, 450 µA with 100 msec per projection and 400 projections over 360Ê for a total scan time of 10 minutes, as previously described (Pasetto et al., 2018). The isotropic resolution of this protocol is 93 µm. The scanned images were reconstructed in 3D and analyzed using Micro View analysis software (version 2.1.1; GE

Healthcare). We measured the distance from the last cervical vertebra to the last lumbar vertebra (segment AB; Supplementary Fig. 1c) and the perpendicular distance to the dorsal edge of the vertebra at the greatest curvature (segment CD; Supplementary Fig. 1c). The index of kyphosis was defined as the ratio of AB to CD.

Behavioral analysis

In this study both male and female mice were tested, at 6 and 12 months of age. All behavioral tests were carried out at the same time of day, in the afternoon. Mice were allowed to habituate to the test room for at least 1h. Test environments were thoroughly cleaned between test sessions and males were tested before females. Open field, three-chamber sociability test, Morris Water Maze and Novel Object Recognition Test used Ethovision XT, 5.0 software (Noldus Information Technology, Wageningen, The Netherlands) to record the parameters.

Body weight

Mice were weighed once every 15 days, at the same time of day, in the afternoon, on a balance with readability0.1 g and linearity ± 0.3 g (EU-C 7500PT, Gibertini).

Open field

The open field consists of a square Perspex box arena with walls (40 x 40 x 40 cm). The “center zone” was defined as a square covering 16% of the total arena area (16 cm x 16 cm central square) and the “periphery zone” as the surrounding border. Each mouse was placed in the center of the arena and velocity, total distance moved and the time spent in the central and periphery zones of the open field was recorded for 5 min.

Elevated plus-maze

The device consisted of a central part (5 x 5 cm), two opposing open arms (30 x 5 cm) and two opposing closed arms (same size) with 14 cm high, non-transparent walls. The maze was elevated 73 cm above the floor. At the beginning of each trial, mice were placed on the central platform, facing an open arm. Their behavior was recorded for 5 min then analyzed by an operator blind to the genotype. Entry into an arm was recorded when the mouse placed its four paws in that arm (Tschenett et al., 2003).

Three-chamber sociability test

The apparatus for the social behavior test consists of three chambers connected with retractable open doorways on two dividing walls. The two external chambers contained an inverted empty wire cup. The test comprised three main steps. After a5 min habituation period, during which the test mouse was allowed to explore the arena freely, an unfamiliar mouse (stranger 1) was introduced into one of the empty wire cups to measure social preference. The time the test mouse spent sniffing each wire cup was recorded for 10 min. then a new mouse (stranger 2) was introduced into the remaining empty wire cup in order to measure social recognition. Time spent sniffing each wire cup was measured. Unfamiliar mice of the same sex and age were used as strangers 1 and 2.

Morris Water Maze

The Morris Water Maze test (MWM) consists of a circular pool (100 cm diameter) filled with water (22°C) made opaque by the addition of nontoxic, odorless white tempera. The escape platform,made of transparent plastic, was placed 1 cm below the water surface. The MWM test involved five days of training and a one-day probe trial. During each day of training mice were placed successively in north, east, south, and west positions, with the escape platform hidden in the middle of the southwest quadrant. Whenever the mice failed to reach the escape platform, they were placed on it for 10 s. Latencies before reaching the platform were recorded in four-trial sessions. After the training, on the sixth day a probe trial was conducted, removing the platform from the pool. Time spent in the previously correct target quadrant (Q1) was measured in a single 1-min trial.

Novel object recognition

The Novel Object Recognition Test (NORT) was done in a square gray arena with walls (40 x 40 x 40 cm). The following objects were used: a black plastic cylinder (4 x 5 cm) and a metal cube (3 x 5 cm). After a5 min habituation trial during which the animal explored the empty arena freely, on the second day mouse was placed in the same arena containing two identical objects. On the last day mouse was again placed in the arena containing the object presented the second day (familiar), together with a new, different one, and the time spent exploring the two objects was recorded for 5 min. The parameter analysed was the discrimination index (DI), defined as: $DI = (T_{New} - T_{Familiar}) / (T_{New} + T_{Familiar})$ where T_{New} is the time spent with the new object and $T_{Familiar}$ the time spent with the familiar object.

Rotarod

Motor performance of the mice was determined using a Rotarod (Ugo Basile) in acceleration mode (7-44 rpm) over 5 min. The mice were given up to three attempts and the longest latency to fall was considered in statistical analysis. Mice were tested at the same time of day, in the afternoon, once every 15 days, from 13 to 22 months of age.

Grid test

Grip strenght was measured using the following score:

$$Score = T_{tot} - \sum_{i}^{n} \frac{T_{double\ i}}{2} - \sum_{j}^{n} \frac{T_{single\ j}}{4}$$

where T_{tot} is the time spent hanging before falling from the grid, n is the number of events in which both hind paws (i) or a fore or a hind paw (j) became detached from the grid, $T_{double\ i}$ is the number of seconds the i-th event lasted, $T_{single\ j}$ is the number of seconds the j-th event lasted, as previously described (Lauranzano et al., 2015).

Hindlimb clasping

Hindlimb clasping was quantified using the following 3-point score: 3, hindlimbs extending to an angle of 120 degrees; 2.5, hindlimbs extending to < 90 degrees with decreased reflex in one limb; 2.0, as 2.5 with decreased reflex in both hindlimbs; 1.5, loss of reflex with marked flexion in one hindlimb; 1, as 1.5 with marked flexion in both hindlimbs; 0.5, loss of reflex with hindlimbs and paws held close to the body. Mice were tested at the same time of day, in the afternoon, once every 15 days, from 13 to 22 months of age.

Real-time PCR

The total RNA from cortex was extracted using the RNeasy® Mini Kit (Qiagen). RNA samples were treated with DNase I and reverse transcription was done with a High Capacity cDNA Reverse Transcription Kit (Life Technologies). For Real-time PCR we used the Taq Man Gene expression assay (Applied Biosystems) following the manufacturer's instructions, on cDNA specimens in triplicate, using 1X Universal PCR master mix (Life Technologies) and 1X mix containing specific receptor probes for *GRN* (Mm00433848_m1; Life Technologies) and *TARDBP* (Mm01257504_g1; Life Technologies). Relative quantification was calculated from the ratio of the cycle number (Ct) at which the signal crossed a threshold set within the logarithmic

phase of the given gene to that of the reference β-actin gene (Mm02619580_g1; Life Technologies). Means of the triplicate results for each animal were used as individual data for $2^{-\Delta\Delta Ct}$ statistical analysis.

Statistical analysis

Prism 7.0 (GraphPad Software Inc., San Diego, CA) was used. For each variable, the differences between experimental groups were analyzed with Student's *t* test or one-way ANOVA followed by Tukey's multiple comparisons test or Uncorrected Fisher's LSD post-hoc test. *P* values below 0.05 were considered significant. All graphs illustrate the mean ± standard error of the mean (SEM).

RESULTS

***PPIA*-/- mice display neuropathological alterations, worsening with age**

In previous studies we found that *PPIA*-/- mice had a higher burden of Triton-insoluble phosphorylated TDP-43 (insoluble pTDP-43) in the ventral horn spinal cord and brain cortex already at four months of age (Lauranzano et al., 2015). We detected no motor neuron loss (Pasetto et al., 2017) and no motor phenotype (Supplementary Fig. 1a-b), but there was a tendency to kyphosis (Supplementary Fig. 1 c). To see whether these were prodromal signs of neurodegeneration, we did a neuropathological analysis of older *PPIA*-/- mice. Quantitative MRI was done longitudinally on *PPIA*-/- and *PPIA*+/+ mice at 6 and 12 months of age. We first observed that brain volume in *PPIA*+/+ mice increased slightly at 12 months of age, while in *PPIA*-/- mice it did not (Fig. 1a). Moreover, *PPIA*-/- mice had a lower total brain volume than controls, with the most marked difference at 12 months (-13%) (Fig. 1a). Next, we verified the effect of PPIA depletion on hippocampus, cortex, frontal cortex and cerebellum, adjusting for total brain volume. MRI showed that *PPIA*-/- mice had a significantly smaller hippocampus than *PPIA*+/+ mice at both 6 and 12 months of age. There was also a reduction of the relative volume with age, independently from the genotype, with a slightly more marked reduction in *PPIA*-/- mice (-21% versus -23%) (Fig. 1b). Cortex volume of *PPIA*-/- mice was also smaller than PPIA+/+ mice, but less so: 5% and 11% smaller respectively at 6 and 12 months of age, but in neither casewas the difference significant (p=0.07 at 12 months) (Fig. 1c). Nonetheless, *PPIA*-/- mice presented significant cortex atrophy at 12 compared to 6 months of age (-14%), not present in control mice. In contrast, the frontal cortex and cerebellum relative volumes did not significantly differ in *PPIA*-/- mice

and controls and did not change with age (Fig. 1d-e). To investigate whether brain atrophy reflects neuronal loss we did a histological analysis on the hippocampus and cortex. In agreement with MRI data, there were substantially fewer Nissl-positive neurons in the hippocampus CA1 region of *PPIA*-/- mice than in controls at 6 and 12 months of age, with a tendency to be more pronounced at 12 months (Fig. 2a). In the cortex *PPIA*-/- mice had significantly fewer Nissl-positive neurons than controls at 6 and 12 months of age (Fig. 2b). They also had significantly greater neuron loss at 12 months, similarly to MRI data.

We next evaluated the glial response in the hippocampus and cortex of *PPIA*-/- mice. In the hippocampus, PPIA deficiency increased astroglial activation at 12 months of age (Fig. 2c), but had no effect on microglia (Fig. 2d). In the cortex, PPIA deficiency did not affect either astroglia or microglia (Supplementary Fig. 2a-b). Thus, *PPIA*-/- mice display neuropathological features that reflect neuronal loss in both the hippocampus and cortex, and worsen with age.

TDP-43 pathology in cortex and hippocampus of *PPIA*-/- mice

To explore whether the neuropathological alterations were associated with TDP-43 pathology, we did biochemical and immunohistochemistry analyses for TDP-43 in brains of *PPIA*-/- mice and controls at 6 and 12 months of age (Fig. 3, Supplementary Fig. 3). Using a biochemical approach, we detected in the cortex of 6 month-old *PPIA*-/- mice a significant increase in pTDP-43 in the cytoplasm and a concomitant decrease of TDP-43 in the nucleus compared to controls (Fig. 3n). TDP-43 cytoplasmic mislocalization was seen specifically in the pathological tissue, as we saw no change in TDP-43 subcellular localization in cerebellum (Supplementary Fig. 3a).

We analyzed the Triton-insoluble protein fraction from brain cortex of *PPIA*-/- and *PPIA*+/+ mice by dot blot analysis and found that in *PPIA*-/- mice there was significantly larger amount of insoluble and ubiquitinated proteins, TDP-43 and pTDP-43 (Supplementary Fig. 3b-e), features that were already clear at four months of age (Lauranzano et al., 2015). We also analyzed other proteins associated with ALS/FTD that are prone to aggregation (SOD1, FUS, hnRNPA2/B1) and interact with TDP-43 in RNP complexes and/or stress granules (hnRNPA2/B1, TIA1) (Supplementary Fig. 3f-i). In the absence of PPIA, there was a higher level of insoluble hnRNPA2/B1 and TIA1 (Supplementary Fig. 3f-g), but no change in the level of insoluble FUS (Supplementary Fig. 3h), indicating the involvement of PPIA in hnRNP complexes/TDP-43-related

mechanisms, and a possible dissociation from FUS-related mechanisms. In addition in *PPIA-/-* brain cortex there was a more than two-fold increase in insoluble SOD1 (Supplementary Fig. 3i), confirming the likely function of PPIA as a chaperone of SOD1 (Lauranzano et al., 2015).

Finally, we examined TDP-43 fragmentation in insoluble and soluble brain cortex fractions (Supplementary Fig. 3j). As expected, 35- and 25-kDa TDP-43 fragments were abundant, mainly in the insoluble fraction. While TDP-43 bands at 43 and 35 kDa did not change in *PPIA-/-* and *PPIA+/+* mice (data not shown), the 25-kDa TDP-43 fragment rose significantly with PPIA depletion, suggesting a role for PPIA in TDP-43 stability.

At 12 months of age, histopathological analysisindicated a widespread TDP-43 signal in different brain regions of *PPIA-/-* mice, with higher intensity in hippocampus and cortex (Fig. 3a-b). In the hippocampus of *PPIA-/-* mice there were TDP-43 neuronal cytoplasmic inclusions in the pyramidal layer of CA3 and CA1 (Fig. 3c, d), in the granule cell layer of dentate gyrus (Fig. 3e), the stratum radiatum of CA1 (Fig. 3f) and the stratum oriens of CA3 and CA1 (Fig. 3g, h). Inclusions took different shapes, skein-like compact (Fig. 3c-e), round (Fig. 3f, g) and filamentous (Fig. 2g, h). *PPIA-/-* mice had diffuse TDP-43 neuronal cytoplasmic inclusions also in the somatosensory (Fig. 2i, j, l, m) and temporal cortex (Fig. 2k). Inclusions in the cortex were more abundant and aggregate in compact skein-like and round formations.

We confirmed the presence of TDP-43 inclusions in *PPIA-/-* brain regions using a pTDP-43 antibody that does not react with physiological nuclear TDP-43 but identifies only pathological brain lesions (Fig. 4) (Tan et al., 2013). *PPIA-/-* mice had diffuse pTDP-43 inclusions (Fig. 4f-t), not observed in *PPIA+/+* mice (Fig. 4a-e). In particular, in the somatosensory (Fig. 4f, g) and auditory-temporal cortex (Fig. 4h-k) there were pTDP-43 granular, skein-like and round compact inclusions. The signal was even larger in hippocampus, where pTDP-43 inclusions were more abundant, with a compact aggregated round shape (Fig. 4l-t). Hippocampus nuclear cytoplasmic inclusions were widespread in the CA1 pyramidal layer (Fig. 4l, m), in stratum radiatum of CA3 (Fig. 4p-r), stratum oriens of CA1 (Fig. 4n, o) and subiculum (Fig. 4s, t).

We can therefore confirm that PPIA deficiency induces a clear-cut neuropathological phenotype in the brain of the mice, with marked TDP-43 pathology and other alterations related to RNA metabolic pathways.

PPIA-/- mice have defects in synaptic plasticity

To assess whether the structural deficit of the brain regions and the TDP-43 pathology lead to synaptic impairment, we first measured the levels of synaptophysin and PSD95, markers of pre- and post-synaptic structures, in the cortex of *PPIA*-/- mice and controls at 6 and 16 months of age (Fig. 5 a-b). There were age-related reductions of both PSD95 and synaptophysin, more marked in *PPIA*-/- than *PPIA*+/+ mice (Fig. 5 a-b).

Next, we made extracellular field recordings of excitatory postsynaptic potentials (fEPSPs) in the CA1 hippocampal region of *PPIA*-/- mice at 16 months of age compared to controls. Long-term potentiation (LTP) induced with theta burst stimulation (TBS) had a smaller amplitude in *PPIA*-/- mice (Fig. 5c), suggesting an impairment of synaptic plasticity in the hippocampus. In conclusion, the results in hippocampus and cortex suggest an involvement of PPIA in the architecture and functional of the synapse.

PPIA-/- mice present cognitive and behavioral but no motor and memory impairments

We checked whether PPIA deficiency, besides compromising neuronal functions, promotes cognitive and motor impairment. We used *PPIA*-/- mice on a C57BL/6J genetic background, as they are more responsive to cognitive tests than 129Sv mice (Brooks et al., 2005). We verified that *PPIA*-/- C57BL/6J mice also display TDP-43 pathology. TDP-43 mislocalized to the cytoplasm in the cortex (Supplementary Fig. 4a), but not cerebellum (Supplementary Fig. 4b), and accumulated in the insoluble fraction (Supplementary Fig. 4c-e).

PPIA-/- mice showed no exploratory abnormalities, as they spent the same time as *PPIA*+/+ mice in the inner zone in the open field test, at both 6 and 12 months of age (Fig. 6a). In the elevated plus maze paradigm *PPIA*-/- mice showed less anxiety and more disinhibition as they spent twice the time in the open arms compared with controls (Fig. 6b). This behavior is lost with time, as at 12 months of age *PPIA*-/- mice spent the same time as controls in open arms (Fig. 6b).

We used the three-chamber test to examine sociability and social memory in *PPIA*-/- mice. *PPIA*-/- mice at 6 months of age spent twice the time of controls sniffing the stranger than the empty cage (Fig. 6c), suggesting a more social attitude. However, at 12 months of age *PPIA*-/- mice changed their behavior,

spending the same time with the stranger and the empty cage and, comparing with mice at 6 months of age, they spent significantly less time sniffing the stranger (Fig. 6c).

Combining the results of the elevated plus maze and the three-chamber tests, we suggest that the increased social attitude of *PPIA*-/- mice may be the consequence of increased disinhibition. During the social recognition memory task, which requires normal hippocampal function, *PPIA*-/- mice at 6 months of age distinguish the stranger mouse (Stranger 2) from the familiar one (Stranger 1) (Fig. 6d), suggesting a normal social memory. However, at 12 months they no longer distinguish the novel mouse from the familiar one, suggesting social impairment and hippocampal dysfunction (Fig. 6d).

To investigate the role of impaired hippocampus in *PPIA*-/- mice further, we used the Morris water maze (MWM) and novel object recognition (NORT) tests. Surprisingly, *PPIA*-/- and control mice showed no differences in the time spent in the target quadrant for the MWM (Fig. 6e) and in their DI in the NORT (Fig. 6f), suggesting no memory impairment. We also characterized the involvement of the amygdala, evaluating hindlimb clasping in mice. *PPIA*-/- mice presented more clasping events than controls, particularly in the last six months of life (Fig. 6g), suggesting later impairment of amygdala functions.

We observed no motor impairment in *PPIA*-/- mice, assessed in the rotarod test and grid tests (Supplementary Fig. 5 a-b). This result correlates with the absence of motor neuron loss in the lumbar spinal tract of *PPIA*-/- mice up to 12 months of age (Supplementary Fig. 5 c-d). Finally, there was a reduction in the survival of *PPIA*-/- mice compared to *PPIA*+/+ mice of more than four months (702 ± 90 days versus 837 ± 107 days) (Fig. 6h).

In summary, *PPIA*-/- present cognitive and behavioral impairments reminiscent of bvFTD.

***PPIA* deficiency downregulates *GRN* and *TARDBP* expression**

In previous work we demonstrated that PPIA deficiency affected the expression of a number of TDP-43 target genes, including *GRN*, which is a major mutated gene in familiar FTD (Lauranzano et al., 2015). *GRN* mutations in patients result in haplo-insufficiency and *GRN* knock-out mice present an FTD-like phenotype with mild TDP-43 pathology (Solomon et al., 2019). We verified whether knocking out *PPIA* influenced *GRN* expression in the brain cortex of the mice. *GRN* mRNA levels were slightly but significantly reduced in *PPIA*-/- mice compared to controls (Fig. 7a).

TDP-43 downregulation and overexpression are both highly toxic for neurons and in fact, physiological TDP-43 levels are tightly controlled (Ayala et al., 2011; Polymenidou et al., 2011). We found that TDP-43 at RNA and protein levels were slightly lower in *PPIA*-/- mice than controls (Fig. 7b-c), suggesting that PPIA deficiency may interfere with the mechanisms of TDP-43 auto-regulation and contribute to neuron vulnerability. In conclusion, PPIA deficiency affects multiple genes and pathways that are FTD-relevant, indicating a central role in brain processes and functions.

DISCUSSION

PPIA is a multifunctional protein abundantly expressed by neurons in the brain (Göldner and Patrick, 1996; Ryffel et al., 1991). It is a foldase and a molecular chaperone with scaffolding properties (Fischer et al., 1989; Lauranzano et al., 2015). Both protective and detrimental biological activities have been attributed to PPIA in different cell types and diseases (Hoffmann and Schiene-Fischer, 2014; Nigro et al., 2013), but its role in the brain is still not clear. In previous work we found that PPIA is a TDP-43 interactor that governs key TDP-43 functions and is altered in animal models and patients with ALS (Filareti et al., 2017; Lauranzano et al., 2015; Luotti et al., 2020; Nardo et al., 2011). Here, we further explore PPIA's functions in the brain by deep characterization in *PPIA*-/- mice. These mice develop a neurodegenerative disease that is very similar to bvFTD with TDP-43 pathology, indicating that PPIA has a dominant protective effect against neurodegeneration in the brain and if dysfunctional, it may have a central role in the development of TDP-43 related pathologies.

The main neuropathological trait of FTD in patients is degeneration of the frontal and/or temporal cortices. In *PPIA*-/- mice, MRI analysis did not detect atrophy of the frontal cortex. This was not surprising, since the frontal cortex in mice is much less developed than in humans, and not easily comparable anatomically and functionally (Brown and Bowman, 2002). However, when we considered the whole cortex, progressive cortical atrophy was clearly detected in mice, paralleling the progressive degeneration of the hippocampus. Although traditionally described as a characteristic of Alzheimer's disease (AD), hippocampal degeneration is also common in FTD patients (Lindberg et al., 2012; Rohrer et al., 2015). In *PPIA*-/- mice the correlation between the extent of atrophy and neuronal loss detected histopathologically in cortex and

hippocampus corroborated the MRI results. The absence of atrophy and neuron loss in cerebellum confirmed a key role of PPIA in specific brain regions.

In FTD patients, the compromised brain architecture leads to behavior, personality and/or language impairments, with some preservation of memory (McKhann et al., 2001). In *PPIA*-/- mice, a battery of behavioral and cognitive tests detected disinhibition, loss of empathy, with consequent social disinterest, but no memory impairment. The resulting picture closely resembles the main features of bvFTD (Rascovsky et al., 2011). In *PPIA*-/- mice the behavioral symptoms follow a peculiar course. Initially, they present disinhibition with no social impairment, and later they show loss of disinhibition and develop apathy and social disinterest. Interestingly, while most patients with bvFTD display both disinhibition and apathy during the course of the disease, some may initially present as primarily disinhibited or primarily apathetic (Le Ber et al., 2006).

Despite the hippocampal degeneration, we did not see any memory impairment in the Morris water maze test or object recognition task. However, these tests were developed to study AD-related memory defects in mice and agreement is lacking on the best tests for FTD models (Vernay et al., 2016). More specific cognitive tasks are probably necessary to explore hippocampal involvement in FTD. In FTD, atrophy of the hippocampus is mainly in the anterior region, while in patients with AD it is diffuse, which possibly explains the different cognitive impairment in the two diseases (Laakso et al., 2000; Lindberg et al., 2012). BvFTD presents motor dysfunction when comorbid with ALS or parkinsonism (Burrell et al., 2011). However, *PPIA*-/- mice had no motor impairment and no motor neuron loss, indicating that PPIA deficiency promotes a pure FTD phenotype.

FTLD-TDP is the most common neuropathologic type of FTLD and presents cellular inclusion bodies composed of TDP-43 (Irwin et al., 2015). In previous work we detected increased detergent-insoluble TDP-43 and pTDP-43 in brain and spinal cord of *PPIA*-/- mice already at four months of age, suggesting TDP-43 inclusion formation and pathology (Lauranzano et al., 2015). Here we deeply characterized TDP-43 pathology in the brain of *PPIA*-/- mice, at different stages of the disease, using various histological and biochemical approaches. Cortex and hippocampus presented diffuse, marked TDP-43 pathology with all the neuropathological features of FTD, such as detergent-insolubility, fragmentation, hyperphosphorylation and cytoplasmic mislocalization/nuclear clearing. C-terminal fragments of TDP-43 are commonly found in FTD

patients and are hallmarks of the pathology in the brain. In most lesions of patients with FTLD-TDP the burden of TDP-43 C-terminal fragments is greater than that of TDP-43 full-length (Josephs et al., 2019). Similarly, in the cortex of *PPIA*-/- mice, the 25-kDa TDP-43 fragment was significantly enriched in the detergent-insoluble fraction, while the full-length was not. Biochemical analysis of the detergent-insoluble fraction of the cortex of *PPIA*-/- mice indicated general increases in insoluble, ubiquitinated proteins and TIA1 stress granule marker, confirming PPIA's involvement in regulating protein homeostasis, as already suggested by other work in this laboratory (Filareti et al., 2017; Luotti et al., 2020). We recently reported that ALS patients have low PPIA levels and a concomitant shift toward increased protein partitioning in the insoluble fraction, with high levels of insoluble TDP-43 and hnRNPA2/B1 (Luotti et al., 2020). hnRNPA2/B1 and SOD1 were also enriched in the detergent-insoluble fraction of *PPIA*-/- mice, while FUS was not. On one hand this confirms that, besides TDP-43, hnRNPA2/B1 and SOD1 are PPIA interactors and client proteins for PPIA folding/refolding activity (Lauranzano et al., 2015). On the other hand, this suggests that the pathway leading to FUS pathology is PPIA-independent, which is consistent with the fact that although FUS and TDP-43 are structurally and functionally very similar PPIA is not a common interactor (Blokhuis et al., 2016; Lauranzano et al., 2015).

Several lines of evidence indicate an important role for neuroinflammation in the progression of FTD (Bright et al., 2019). Microglial activation and astrogliosis have been detected in the frontal and temporal cortices of FTD patients. In *PPIA*-/- mice, we found astrogliosis that increased with age, but no microglial activation. We know that PPIA itself has a role in microglial activation and the neuroinflammatory response by activating the CD147/EMMPRIM receptor, therefore *PPIA*-/- mice are not suitable to investigate this feature of the pathology (Bouybayoune et al., 2019; Pasetto et al., 2017) . However, other mouse models of FTD, *GRN* +/- mice, develop age-dependent social and emotional deficits without gliosis, indicating a dissociation between neuroinflammation and functional deficits (Ahmed et al., 2010; Filiano et al., 2013).

Possible consequences of the neuropathological changes are synaptic malfunction and/or loss of synapses, which seem to be at the basis of neurodegeneration and cognitive impairment in AD. In FTD, downregulation of genes involved in synaptic function has been found in human samples with TDP-43

pathology (Mishra et al., 2007). Moreover, many mRNA TDP-43 targets encode proteins involved in synaptic functions (Sephton et al., 2011). In *PPIA-/-* mice we detected downregulation of synaptic proteins (synaptophysin and PSD95) and impairment of synaptic plasticity in hippocampus, indicating that PPIA deficiency also has an effect on synaptic structure and function, possibly contributing to neurodegeneration.

In a previous work, we reported that PPIA governs key TDP-43 functions, such as gene expression regulation (Lauranzano et al., 2015). In fact, knocking down PPIA affected the expression of a number of TDP-43 target genes involved in pathways leading to neurodegeneration, including *GRN*. *GRN* has been found mutated in familial forms of FTD and the disease mechanism seems to be linked to *GRN* haplo-insufficiency, as also confirmed in mouse models (Solomon et al., 2019). In the cortex of *PPIA-/-* mice, we found that *GRN* was downregulated, indicating that a *GRN* loss-of-function probably contributes to the development of an FTD phenotype in *PPIA-/-* mice.

In ALS/FTD patients, TDP-43-induced neurotoxicity quite likely results from a combination of gain of toxic functions, exerted by TDP-43 inclusions, and loss of normal TDP-43 functions (Gendron et al., 2010). In *PPI-/-* mice, in addition to marked, diffuse TDP-43 pathology, we detected TDP-43 downregulation at both the RNA and protein levels. TDP-43 physiological levels are tightly controlled by an auto-regulatory mechanism, which keeps the intracellular level of TDP-43 within a narrow range (Ayala et al., 2011; Polymenidou et al., 2011). This is necessary for TDP-43's role in RNP complexes that may become dysfunctional if the stoichiometry between TDP-43 and the other protein/RNA components is disrupted (Lauranzano et al., 2015). Thus PPIA deficiency not only destabilizes RNP complexes, but also probably impairs the TDP-43 auto-regulatory mechanism, leading overall to a low functional TDP-43 concentration. If complete ablation of TDP-43 is embryonically lethal, conditional knock-out and limited knocking-down of TDP-43 results in neuron degeneration (Iguchi et al., 2013; Mitra et al., 2019; Wu et al., 2012).

In conclusion, the *PPIA-/-* mouse develops a neurodegenerative disease expressing most of the molecular, neuropathological and clinical features of FTD and to our knowledge is the most complete experimental model of pure bvFTD associated with TDP-43 pathology, which is a common phenotype in FTD patients. All animal models of FTD, targeting pathogenic genes such as *TARDBP*, *C9orf72*, *MAPT* and *GRN*, lack some FTD features or present a mixed ALS/FTD phenotype (Tan et al., 2017).

This study provides additional evidence of a key role of PPIA in the central nervous system. PPIA is a multifunctional protein with a wide protein interactome network, implying an involvement in many cellular processes, intracellularly and extracellularly, with both protective and detrimental effects (Lauranzano et al., 2015; Pasetto et al., 2017). In neurons, intracellular PPIA (iPPIA) is mainly protective thanks to its activity as a foldase and a molecular chaperone, and its scaffolding properties. In the central nervous system, extracellular PPIA (ePPIA) has detrimental functions through the interaction with its CD147/EMMPRIN receptor, which can induce an aberrant inflammatory response (Pasetto et al., 2017). We hypothesize that iPPIA and ePPIA are in dynamic equilibrium, in which the prevalence of ePPIA over iPPIA translates into a pathological condition. In ALS we reported that iPPIA is sequestered into aggregates in mice and in patients, resulting in a low intracellular concentration, whereas ePPIA is increasingly secreted (Filareti et al., 2017; Luotti et al., 2020; Massignan et al., 2007; Pasetto et al., 2017). We showed that selective pharmacological inhibition of ePPIA is enough to protect motor neurons, reduce neuroinflammation and consequently increase survival in the $SOD1^{G93A}$ mouse model of ALS (Pasetto et al., 2017). We also showed that ePPIA is selectively toxic toward motor neurons, but has no effect on cortical and cerebellar granule neurons. The absence of motor dysfunction in *PPIA-/-* mice can be easily explained by the lack of ePPIA toxicity to which motor neurons are particularly susceptible. Therefore, the neurodegenerative disease in *PPIA -/-* mice is due to the lack of the dominant protective effect of iPPA in the brain, which is quite likely linked to its regulatory effect on TDP-43 and its multiple mRNA targets. Considering that an impaired interaction of TDP-43 with PPIA has been observed in ALS/FTD patients (Lauranzano et al., 2015), further studies are now warranted to investigate whether this could be an interesting therapeutic target not only for FTD, but also for ALS/FTD.

In conclusion, our findings indicate that PPIA is involved in multiple genes and pathways that have central roles in brain processes and is fundamental for TDP-43 functions. *PPIA-/-* mice recapitulate all the key features of bvFTD associated with TDP-43 pathology. Thus the *PPIA-/-* mouse is a useful experimental model to investigate the mechanisms of FTD, and possibly of other TDP-43 proteinopathies, with a view to developing novel therapeutic approaches.

ACKNOWLEDGMENTS

This work was supported by grants from the "Fondazione Regionale per la Ricerca Biomedica di Regione Lombardia", project TRANS-ALS (to V.B.) and ERA-Net for Research Programmes on Rare Diseases, project MAXOMOD (to V.B.). We thank Bradford C. Berk and Patrizia Nigro for providing the *PPIA*-/- mice on C57BL/6J genetic background. We thank Judith Baggott for editorial assistance.

FIGURE LEGENDS

Figure 1 Brain atrophy worsens with age in *PPIA*-/- mice. The volume of total brain (**a**), hippocampus (**b**), cortex (**c**), frontal cortex (**d**) and cerebellum (**e**) was measured using quantitative MRI analysis in *PPIA*+/+ and -/- mice, at 6 (6 mo) and 12 (12 mo) months of age. Right panels are representative MRI images of *PPIA*+/+ and -/- brain regions at 12 months of age. The white dashed line represents the ROI considered for MRI quantification. Scale bar 1 mm. (**b-e)** The volume of hippocampus, cortex, frontal cortex and cerebellum was adjusted for total brain volume and data are expressed as relative volume. (**a-e)** Mean ± SEM (n=5, 6 months; n=6, 12 months). *$p < 0.05$, *PPIA* -/- versus *PPIA*+/+ mice and $^{\#}p < 0.05$, 6 months versus 12 months of age, by one-way ANOVA, Tukey's post hoc test.

Figure 2 Depletion of PPIA induces progressive neuron loss and astrogliosis. (**a, b)** Neurons in CA1 region and cortex were counted in *PPIA*+/+ and -/- mice at 6 and 12 months of age. Representative Nissl-stained brain section are shown. Scale bar 50 µm. Mean ± SEM (n=5, CA1 region; n=4, cortex). (**c)** GFAP-immunostaining in hippocampus was quantified in *PPIA*+/+ and -/- mice at 6 and 12 months of age. Representative GFAP-stained brain sections are shown. Scale bar 50 µm. Mean ± SEM (n=4, *PPIA*+/+; n=5, *PPIA*-/-). (**d)** Iba-1 immunostaining in hippocampus was quantified in *PPIA*+/+ and -/- mice at 6 and 12 months of age. Representative Iba-1-stained brain sections are shown. Scale bar 50 µm. Mean ± SEM (n=5, 6 months; n=4, 12 months). *$p < 0.05$ versus the respective *PPIA*+/+ mice and $^{\#}p < 0.05$ versus the respective 6 months, by one-way ANOVA, Tukey's post hoc test **(a, d)** and Uncorrected Fisher's LSD post hoc test **(b, c)**.

Figure 3 Diffuse TDP-43 inclusions in hippocampus and cortex of *PPIA*-/- mice. (**a, b)** Diffuse TDP-43 immunostaining was observed in brains of *PPIA*-/- mice at 12 months of age compared to *PPIA*+/+. Scale

bar 1 mm.(**c-h)** In hippocampus of *PPIA*-/- mice, TDP-43 inclusions were observed in the pyramidal layer of CA3 and CA1 (**c, d**), in the granule cell layer of dentate gyrus (**e**), in stratum radiatum of CA1 (**f**) and in stratum oriens of CA3 and CA1 (**g, h**). (**c-g)** Scale bar 20 µm. (**h)** Scale bar 50 µm. (**i-m)** In *PPIA*-/- mice TDP-43 inclusions were observed in the somatosensory (**i, j, l, m**) and temporal cortex (**k**). Scale bar 20 µm. (**n)** Equal amounts of cytoplasmic and nuclear fractions from cortex of *PPIA*+/+ and -/- mice at 6 months of age were analyzed by WB for TDP-43 or pTDP-43. Immunoreactivity was normalized to protein loading. Data (mean ± SEM, n=5) are percentages of immunoreactivity in *PPIA*+/+ mice in the respective fraction (RI, relative immunoreactivity). *$p < 0.05$ versus *PPIA*+/+ mice Student's t-test.

Figure 4 Accumulation of pTDP-43 inclusions in brain of *PPIA*-/- mice. pTDP-43 immunostaining was analyzed in cortex of *PPIA*+/+ (**a, b**) and *PPIA*-/- (**f-k**) mice at 12 months of age. pTDP-43 staining was observed in the somatosensory (**f, g**) and auditory-temporal (**h-k**) cortex. **g, i, k** are magnified imagines of the dashed area in figures **f, h, j**. Hippocampus of *PPIA*-/- mice (**l-t**) show ven more marked pTDP-43 staining than *PPIA*+/+ mice (**c-e**). pTDP-43 inclusions are widespread in the CA1 pyramidal layer (**l, m**), stratum oriens of CA1 (**n, o**), stratum radiatum of CA3 (**p-r**) and subiculum (**s, t**). or: stratum oriens; rad: stratum radiatum; sub: subiculum. **m, o, q, r, t** are magnified imagines of the dashed area in **l, n, p, s**. Scale bar 50 µm: **a-f, h, j, l, n, p, s.** Scale bar 20 µm: **g, i, k, m, o, q, r, t.**

Figure 5 *PPIA*-/- mice display defects in synaptic plasticity. (**a, b)** Dot blot analysis of lysates from cortex of PPIA+/+ and -/- mice at 6 and 16 months of age. Immunoreactivity was normalized to protein loading. Data (mean ± SEM, n=5) are percentages of immunoreactivity in PPIA+/+ mice at 6 months of age (RI, relative immunoreactivity).*$p < 0.05$ versus the respective *PPIA*+/+ mice and $^{\#}p < 0.05$ versus the respective 6 months, by one-way ANOVA, Tukey's post hoc test **(a)** and Uncorrected Fisher's LSD post hoc test **(b)**. (**c)** CA1 LTP induced with theta burst stimulation (TBS) is reduced in *PPIA*-/- (white rectangle) compared to PPIA+/+ mice (black circle). Data were analyzed with two-way ANOVA for repeated measures, $p < 0.05$ (n=5). Insets show representative traces before and after TBS recorded in slices from *PPIA*+/+ and *PPIA*-/- mice.

Figure 6 *PPIA-/-* mice display behavioral but not memory deficits. (**a)** Open Field: *PPIA-/-* and +/+ mice spent similar time in the inner zone both at 6 (n=10 *PPIA*+/+ and *PPIA-/-*) and 12 months of age (n=10 *PPIA*+/+, n=8 *PPIA-/-*). **(b)** Elevated plus maze: *PPIA-/-* mice spent more time than controls in open arms (n=10 PPIA+/+ and -/- at 6 months, n=8 *PPIA*+/+ and n=5 *PPIA-/-* at 12 months) at 6, but not at 12 months of age. (**c-d)** Three-chamber sociability test. In the sociability trial **(c)**, *PPIA-/-* mice spent more time than controls sniffing Stranger 1 than Empty cage at 6, but not 12 months of age. In the social memory trial **(d)**, *PPIA-/-* mice spent more time sniffing Stranger 2 than Stranger 1, compared to controls, at 6, but not at 12 months of age (n=10 *PPIA*+/+ and -/- at 6 months, n=10 *PPIA*+/+ and n=8 *PPIA-/-* at 12 months). (**e)** Morris water maze: *PPIA-/-* and +/+ mice spent similar time in the target quadrant (Q1) both at 6 (n=10 *PPIA*+/+ and *PPIA-/-*) and 12 (n=10 *PPIA*+/+, n=8 *PPIA-/-*) months of age. **(f)** Novel object recognition test: PPIA-/- and +/+ mice had similar discrimination indexes (DI) at 6 (n=8 *PPIA*+/+ and *PPIA-/-*) and 12 (n=8 *PPIA*+/+, n=5 *PPIA-/-*) months of age. **(g)** Hindlimb clasping: *PPIA-/-* mice clasp hindlimb more frequently than controls (n=13 *PPIA*+/+, n=14 *PPIA-/-*). Mean ± SEM. *p < 0.05 by two-way ANOVA, Bonferroni's post hoc test. **(h)** Kaplan-Meier curve for survival of *PPIA*+/+ (n=13) and *PPIA-/-* mice (n=14). Log-rank Mantel-Cox test for comparing *PPIA*+/+ and -/- mice. (**a-f)** Mean ± SEM. *p < 0.05 versus the respective *PPIA*+/+ mice and $^{\#}$p < 0.05 versus the respective 6 month-old control by one-way ANOVA, Tukey's post hoc test (**a, e, f**) and Uncorrected Fisher's LSD post hoc test (**b, c, d**).

Figure 7 PPIA deficiency downregulated *GRN* and TDP-43. **a-c** Real-time PCR for *GRN* (**a**) and *TARDBP* (**b**) mRNA transcripts and (**c)** dot blot analysis for TDP-43 total protein level, in cortex of *PPIA*+/+ and *PPIA-/-* mice at 6 months of age. (**a-b)** Data are normalized to β-actin and expressed as the mean ± SEM (n=5) fold change ratio; (**c)** data normalized to protein loading. *p < 0.05 versus *PPIA*+/+ mice, Student's t-test.

Supplementary Fig. 1 *PPIA-/-* mice display no motor phenotype, but have a tendency to kyphosis at four months. *PPIA*+/+ (n=10) and *PPIA-/-* (n=14) mice show a similar motor phenotype in Rotarod (**a**) and grid tests (**b**) up to 20 weeks of age. Data (mean ± SEM) are expressed as percentage of maximum performance and were analyzed by two-way ANOVA, Bonferroni's post hoc test. (**c)** Micro-CT analysis shows only a

tendency to kyphosis in *PPIA*-/- mice compared to controls, at four months of age. Kyphosis was evaluated as the ratio between the distance from the last cervical vertebra to the last lumbar vertebra (segment AB) and the perpendicular distance to the dorsal edge of the vertebra at the greatest curvature (segment CD), as shown in the micro-CT images. Data are mean ± SEM (n=6) and were analyzed with Student's t-test.

Supplementary Fig. 2 Absence of astrogliosis and microgliosis in cortex of *PPIA*-/- mice. (**a, b)** Dot blot analysis of GFAP and Iba-1 in cortex of *PPIA*+/+ and -/- mice at 6 and 12 months of age. *PPIA*-/- mice show similar level of GFAP (**a**) and Iba-1 (**b**) as *PPIA*+/+ mice. Immunoreactivity was normalized to protein loading. Data (mean ± SEM, n=4) are percentages of immunoreactivity in PPIA+/+ mice (RI, relative immunoreactivity) and were . analyzed with one-way ANOVA, Tukey's post hoc test.

Supplementary Fig. 3 TDP-43 pathology and alterations in other RNA binding proteins in *PPIA*-/- mice. (**a)** Equal amounts of cytoplasmic and nuclear fractions from cerebellum of *PPIA*+/+ and -/- mice at six months of age were analyzed for TDP-43 or pTDP-43. Immunoreactivity was normalized to protein loading. Data (mean ± SEM, n=5) are percentages of immunoreactivity in PPIA+/+ mice in the respective fraction (RI, relative immunoreactivity) and were analyzed with Student's t-test. (**b)** Analysis of the total TIF from cortex of *PPIA*+/+ and -/- mice, at six months of age. Total TIF is the amount of TIF isolated from the specific tissue and is the ratio of TIF to soluble proteins. Data (mean ± SEM, n=5) are percentages of immunoreactivity in *PPIA*+/+ mice. *p < 0.05 Student's t test. (**c-i)** The levels of insoluble ubiquitin (**c**), TDP-43 (**d**), pTDP-43 (**e**), hnRNP A2/B1(**f**), TIA1 (**g**), FUS (**h**), SOD1 (**i**) in cortex of *PPIA*+/+ and -/- mice, at six months of age were measured by dot blot with the specific antibodies. Immunoreactivity was normalized to protein loading. Data (mean ± SEM, n=5) are percentages of immunoreactivity in *PPIA*+/+ mice. *p < 0.05, Student's t test. (**j)** TDP-43 was also analyzed and characterized by WB. Representative WB of TDP-43 in soluble and insoluble fractions from cortex of *PPIA*+/+ and -/- mice, at six months of age are shown. Data (mean ± SEM, n=5) are percentages of immunoreactivity in *PPIA*+/+ insoluble fraction. *p < 0.05 versus the respective *PPIA*+/+ mice by one-way ANOVA, Tukey's post hoc test

Supplementary Fig. 4 *PPIA*-/- C57BL/6J mice present TDP-43 pathology. Equal amounts of cytoplasmic

and nuclear fractions from cortex (**a**) and cerebellum (**b**) of *PPIA*+/+ and -/- mice on a C57BL/6J background at six months of age were analyzed for TDP-43 or pTDP-43 by dot blot. Immunoreactivity was normalized to protein loading. (**c)** Analysis of the total TIF from cortex of *PPIA*+/+ and -/- mice at six months of age. Total TIF is the amount of TIF isolated from the specific tissue and is the ratio of TIF to soluble proteins. The levels of insoluble TDP-43 (**d**) and pTDP-43 (**e**) in cortex of *PPIA*+/+ and -/- mice at six months of age were measured by dot blot with the specific antibodies. Immunoreactivity was normalized to protein loading. (**a-e)** Data (mean ± SEM, n=4) are percentages of immunoreactivity in *PPIA*+/+ mice. *p < 0.05, Student's t test.

Supplementary Fig. 5 *PPIA*-/- mice present no motor dysfunction. Rotarod test (**a**) and grid test (**b**) show a similar motor phenotype in *PPIA*+/+ (n=13) and *PPIA*-/- (n=14) mice up to 22 months. Data (mean ± SEM) are expressed as percentages of maximum performance and were analyzed by two-way ANOVA and Bonferroni's post hoc test. *PPIA*-/- and *PPIA*+/+ mice present similar numbers of motor neurons, at 4 (**c**) and 12 (**d**) months of age. Nissl-stained motor neurons (MNs > 250 μm^2) were analyzed in lumbar spinal cord. Data (mean ± SEM, n=4) were analyzed with Student's t test.

REFERENCES

Ahmed, Z., Sheng, H., Xu, Y., Lin, W.-L., Innes, A.E., Gass, J., Yu, X., Hou, H., Chiba, S., Yamanouchi, K., et al. (2010). Accelerated Lipofuscinosis and Ubiquitination in Granulin Knockout Mice Suggest a Role for Progranulin in Successful Aging. Am. J. Pathol. *177*, 311–324.

Ayala, Y.M., De Conti, L., Avendaño-Vázquez, S.E., Dhir, A., Romano, M., D'Ambrogio, A., Tollervey, J., Ule, J., Baralle, M., Buratti, E., et al. (2011). TDP-43 regulates its mRNA levels through a negative feedback loop. EMBO J. *30*, 277–288.

Basso, M., Samengo, G., Nardo, G., Massignan, T., D'Alessandro, G., Tartari, S., Cantoni, L., Marino, M., Cheroni, C., De Biasi, S., et al. (2009). Characterization of Detergent-Insoluble Proteins in ALS Indicates a Causal Link between Nitrative Stress and Aggregation in Pathogenesis. PLoS ONE *4*, e8130.

Blokhuis, A.M., Koppers, M., Groen, E.J.N., van den Heuvel, D.M.A., Dini Modigliani, S., Anink, J.J., Fumoto, K., van Diggelen, F., Snelting, A., Sodaar, P., et al. (2016). Comparative interactomics analysis of different ALS-associated proteins identifies converging molecular pathways. Acta Neuropathol. (Berl.) *132*, 175–196.

Boulos, S., Meloni, B.P., Arthur, P.G., Majda, B., Bojarski, C., and Knuckey, N.W. (2007). Evidence that intracellular cyclophilin A and cyclophilin A/CD147 receptor-mediated ERK1/2 signalling can protect neurons against in vitro oxidative and ischemic injury. Neurobiol Dis *25*, 54–64.

Bouybayoune, I., Comerio, L., Pasetto, L., Bertani, I., Bonetto, V., and Chiesa, R. (2019). Cyclophillin A deficiency accelerates RML-induced prion disease. Neurobiol. Dis. *130*, 104498.

Bright, F., Werry, E.L., Dobson-Stone, C., Piguet, O., Ittner, L.M., Halliday, G.M., Hodges, J.R., Kiernan, M.C., Loy, C.T., Kassiou, M., et al. (2019). Neuroinflammation in frontotemporal dementia. Nat. Rev. Neurol. *15*, 540–555.

Brooks, S.P., Pask, T., Jones, L., and Dunnett, S.B. (2005). Behavioural profiles of inbred mouse strains used as transgenic backgrounds. II: cognitive tests. Genes Brain Behav. *4*, 307–317.

Brown, V.J., and Bowman, E.M. (2002). Rodent models of prefrontal cortical function. Trends Neurosci. *25*, 340–343.

Burrell, J.R., Kiernan, M.C., Vucic, S., and Hodges, J.R. (2011). Motor Neuron dysfunction in frontotemporal dementia. Brain *134*, 2582–2594.

Cande, C., Vahsen, N., Kouranti, I., Schmitt, E., Daugas, E., Spahr, C., Luban, J., Kroemer, R.T., Giordanetto, F., Garrido, C., et al. (2004). AIF and cyclophilin A cooperate in apoptosis-associated chromatinolysis. Oncogene *23*, 1514–1521.

Choi, K.J., Piao, Y.J., Lim, M.J., Kim, J.H., Ha, J., Choe, W., and Kim, S.S. (2007). Overexpressed cyclophilin A in cancer cells renders resistance to hypoxia- and cisplatin-induced cell death. Cancer Res. *67*, 3654–3662.

Colgan, J., Asmal, M., and Luban, J. (2000). Isolation, Characterization and Targeted Disruption of Mouse Ppia: Cyclophilin A Is Not Essential for Mammalian Cell Viability. Genomics *68*, 167–178.

Colgan, J., Asmal, M., Neagu, M., Yu, B., Schneidkraut, J., Lee, Y., Sokolskaja, E., Andreotti, A., and Luban, J. (2004). Cyclophilin A Regulates TCR Signal Strength in CD4+ T Cells via a Proline-Directed Conformational Switch in Itk. Immunity *21*, 189–201.

Coyle-Gilchrist, I.T.S., Dick, K.M., Patterson, K., Vázquez Rodríquez, P., Wehmann, E., Wilcox, A., Lansdall, C.J., Dawson, K.E., Wiggins, J., Mead, S., et al. (2016). Prevalence, characteristics, and survival of frontotemporal lobar degeneration syndromes. Neurology *86*, 1736–1743.

Ferrari, R., Manzoni, C., and Hardy, J. (2019). Genetics and molecular mechanisms of frontotemporal lobar degeneration: an update and future avenues. Neurobiol. Aging *78*, 98–110.

Filareti, M., Luotti, S., Pasetto, L., Pignataro, M., Paolella, K., Messina, P., Pupillo, E., Filosto, M., Lunetta, C., Mandrioli, J., et al. (2017). Decreased Levels of Foldase and Chaperone Proteins Are Associated with an Early-Onset Amyotrophic Lateral Sclerosis. Front. Mol. Neurosci. *10*.

Filiano, A.J., Martens, L.H., Young, A.H., Warmus, B.A., Zhou, P., Diaz-Ramirez, G., Jiao, J., Zhang, Z., Huang, E.J., Gao, F.-B., et al. (2013). Dissociation of frontotemporal dementia-related deficits and neuroinflammation in progranulin haploinsufficient mice. J. Neurosci. Off. J. Soc. Neurosci. *33*, 5352–5361.

Fischer, G., Wittmann-Liebold, B., Lang, K., Kiefhaber, T., and Schmid, F.X. (1989). Cyclophilin and peptidyl-prolyl cis-trans isomerase are probably identical proteins. Nature *337*, 476–478.

Gendron, T.F., Josephs, K.A., and Petrucelli, L. (2010). Review: Transactive response DNA-binding protein 43 (TDP-43): mechanisms of neurodegeneration. Neuropathol. Appl. Neurobiol. *36*, 97–112.

Göldner, F.M., and Patrick, J.W. (1996). Neuronal localization of the cyclophilin A protein in the adult rat brain. J. Comp. Neurol. *372*, 283–293.

Handschumacher, R.E., Harding, M.W., Rice, J., Drugge, R.J., and Speicher, D.W. (1984). Cyclophilin: a specific cytosolic binding protein for cyclosporin A. Science *226*, 544–547.

Hoffmann, H., and Schiene-Fischer, C. (2014). Functional aspects of extracellular cyclophilins. Biol Chem *395*, 721–735.

Iguchi, Y., Katsuno, M., Niwa, J., Takagi, S., Ishigaki, S., Ikenaka, K., Kawai, K., Watanabe, H., Yamanaka, K., Takahashi, R., et al. (2013). Loss of TDP-43 causes age-dependent progressive motor neuron degeneration. Brain *136*, 1371–1382.

Irwin, D.J., Cairns, N.J., Grossman, M., McMillan, C.T., Lee, E.B., Van Deerlin, V.M., Lee, V.M.-Y., and Trojanowski, J.Q. (2015). Frontotemporal lobar degeneration: defining phenotypic diversity through personalized medicine. Acta Neuropathol. (Berl.) *129*, 469–491.

Josephs, K.A., Zhang, Y.-J., Baker, M., Rademakers, R., Petrucelli, L., and Dickson, D.W. (2019). C-terminal and full length TDP-43 specie differ according to FTLD-TDP lesion type but not genetic mutation. Acta Neuropathol. Commun. *7*, 100.

Laakso, M.P., Frisoni, G.B., Könönen, M., Mikkonen, M., Beltramello, A., Geroldi, C., Bianchetti, A., Trabucchi, M., Soininen, H., and Aronen, H.J. (2000). Hippocampus and entorhinal cortex in frontotemporal dementia and Alzheimer's disease: a morphometric MRI study. Biol. Psychiatry *47*, 1056–1063.

Lauranzano, E., Pozzi, S., Pasetto, L., Stucchi, R., Massignan, T., Paolella, K., Mombrini, M., Nardo, G., Lunetta, C., Corbo, M., et al. (2015a). Peptidylprolyl isomerase A governs TARDBP function and assembly in heterogeneous nuclear ribonucleoprotein complexes. Brain *138*, 974–991.

Le Ber, I., Guedj, E., Gabelle, A., Verpillat, P., Volteau, M., Thomas-Anterion, C., Decousus, M., Hannequin, D., Véra, P., Lacomblez, L., et al. (2006). Demographic, neurological and behavioural characteristics and brain perfusion SPECT in frontal variant of frontotemporal dementia. Brain J. Neurol. *129*, 3051–3065.

Lee, J.P., Palfrey, H.C., Bindokas, V.P., Ghadge, G.D., Ma, L., Miller, R.J., and Roos, R.P. (1999). The role of immunophilins in mutant superoxide dismutase-1linked familial amyotrophic lateral sclerosis. Proc Natl Acad Sci U A *96*, 3251–3256.

Lindberg, O., Walterfang, M., Looi, J.C.L., Malykhin, N., Östberg, P., Zandbelt, B., Styner, M., Paniagua, B., Velakoulis, D., Örndahl, E., et al. (2012). Hippocampal Shape Analysis in Alzheimer's Disease and Frontotemporal Lobar Degeneration Subtypes. J. Alzheimers Dis. *30*, 355–365.

Luotti, S., Pasetto, L., Porcu, L., Torri, V., Elezgarai, S.R., Pantalone, S., Filareti, M., Corbo, M., Lunetta, C., Mora, G., et al. (2020). Diagnostic and prognostic values of PBMC proteins in amyotrophic lateral sclerosis. Neurobiol. Dis. 104815.

Mancini, S., Balducci, C., Micotti, E., Tolomeo, D., Forloni, G., Masserini, M., and Re, F. (2017). Multifunctional liposomes delay phenotype progression and prevent memory impairment in a presymptomatic stage mouse model of Alzheimer disease. J. Controlled Release *258*, 121–129.

Massignan, T., Casoni, F., Basso, M., Stefanazzi, P., Biasini, E., Tortarolo, M., Salmona, M., Gianazza, E., Bendotti, C., and Bonetto, V. (2007). Proteomic analysis of spinal cord of presymptomatic amyotrophic lateral sclerosis G93A SOD1 mouse. Biochem. Biophys. Res. Commun. *353*, 719–725.

McKhann, G.M., Albert, M.S., Grossman, M., Miller, B., Dickson, D., Trojanowski, J.Q., and Work Group on Frontotemporal Dementia and Pick's Disease (2001). Clinical and pathological diagnosis of frontotemporal dementia: report of the Work Group on Frontotemporal Dementia and Pick's Disease. Arch. Neurol. *58*, 1803–1809.

Mishra, M., Paunesku, T., Woloschak, G.E., Siddique, T., Zhu, L. (Julie), Lin, S., Greco, K., and Bigio, E.H. (2007). Gene expression analysis of frontotemporal lobar degeneration of the motor neuron disease type with ubiquitinated inclusions. Acta Neuropathol. (Berl.) *114*, 81–94.

Mitra, J., Guerrero, E.N., Hegde, P.M., Liachko, N.F., Wang, H., Vasquez, V., Gao, J., Pandey, A., Taylor, J.P., Kraemer, B.C., et al. (2019). Motor neuron disease-associated loss of nuclear TDP-43 is linked to DNA double-strand break repair defects. Proc. Natl. Acad. Sci. U. S. A. *116*, 4696–4705.

Nardo, G., Pozzi, S., Pignataro, M., Lauranzano, E., Spano, G., Garbelli, S., Mantovani, S., Marinou, K., Papetti, L., Monteforte, M., et al. (2011a). Amyotrophic lateral sclerosis multiprotein biomarkers in peripheral blood mononuclear cells. PLoS One *6*, e25545.

Neumann, M., and Mackenzie, I.R.A. (2019). Review: Neuropathology of non-tau frontotemporal lobar degeneration. Neuropathol. Appl. Neurobiol. *45*, 19–40.

Nigro, P., Pompilio, G., and Capogrossi, M.C. (2013). Cyclophilin A: a key player for human disease. Cell Death Dis *4*, e888.

Olney, N.T., Spina, S., and Miller, B.L. (2017). Frontotemporal Dementia. Neurol. Clin. *35*, 339–374.

Pan, H., Luo, C., Li, R., Qiao, A., Zhang, L., Mines, M., Nyanda, A.M., Zhang, J., and Fan, G.-H. (2008). Cyclophilin A Is Required for CXCR4-mediated Nuclear Export of Heterogeneous Nuclear Ribonucleoprotein A2, Activation and Nuclear Translocation of ERK1/2, and Chemotactic Cell Migration. J. Biol. Chem. *283*, 623–637.

Pasetto, L., Pozzi, S., Castelnovo, M., Basso, M., Estevez, A.G., Fumagalli, S., De Simoni, M.G., Castellaneta, V., Bigini, P., Restelli, E., et al. (2017). Targeting Extracellular Cyclophilin A Reduces Neuroinflammation and Extends Survival in a Mouse Model of Amyotrophic Lateral Sclerosis. J. Neurosci. *37*, 1413–1427.

Pasetto, L., Olivari, D., Nardo, G., Trolese, M.C., Bendotti, C., Piccirillo, R., and Bonetto, V. (2018). Micro-computed tomography for non-invasive evaluation of muscle atrophy in mouse models of disease. PloS One *13*, e0198089.

Polymenidou, M., Lagier-Tourenne, C., Hutt, K.R., Huelga, S.C., Moran, J., Liang, T.Y., Ling, S.C., Sun, E., Wancewicz, E., Mazur, C., et al. (2011). Long pre-mRNA depletion and RNA missplicing contribute to neuronal vulnerability from loss of TDP-43. Nat Neurosci *14*, 459–468.

Rascovsky, K., Hodges, J.R., Knopman, D., Mendez, M.F., Kramer, J.H., Neuhaus, J., van Swieten, J.C., Seelaar, H., Dopper, E.G.P., Onyike, C.U., et al. (2011). Sensitivity of revised diagnostic criteria for the behavioural variant of frontotemporal dementia. Brain J. Neurol. *134*, 2456–2477.

Rein, T. (2020). Peptidylprolylisomerases, Protein Folders, or Scaffolders? The Example of FKBP51 and FKBP52. BioEssays News Rev. Mol. Cell. Dev. Biol. e1900250.

Rohrer, J.D., Nicholas, J.M., Cash, D.M., van Swieten, J., Dopper, E., Jiskoot, L., van Minkelen, R., Rombouts, S.A., Cardoso, M.J., Clegg, S., et al. (2015). Presymptomatic cognitive and neuroanatomical changes in genetic frontotemporal dementia in the Genetic Frontotemporal dementia Initiative (GENFI) study: a cross-sectional analysis. Lancet Neurol. *14*, 253–262.

Ryffel, B., Woerly, G., Greiner, B., Haendler, B., Mihatsch, M.J., and Foxwell, B.M. (1991). Distribution of the cyclosporine binding protein cyclophilin in human tissues. Immunology *72*, 399–404.

Sephton, C.F., Cenik, C., Kucukural, A., Dammer, E.B., Cenik, B., Han, Y., Dewey, C.M., Roth, F.P., Herz, J., Peng, J., et al. (2011). Identification of neuronal RNA targets of TDP-43-containing ribonucleoprotein complexes. J Biol Chem *286*, 1204–1215.

Sherry, B., Yarlett, N., Strupp, A., and Cerami, A. (1992). Identification of cyclophilin as a proinflammatory secretory product of lipopolysaccharide-activated macrophages. Proc Natl Acad Sci U A *89*, 3511–3515.

Solomon, D.A., Mitchell, J.C., Salcher-Konrad, M.-T., Vance, C.A., and Mizielinska, S. (2019). Review: Modelling the pathology and behaviour of frontotemporal dementia. Neuropathol. Appl. Neurobiol. *45*, 58–80.

Tan, R.H., Shepherd, C.E., Kril, J.J., McCann, H., McGeachie, A., McGinley, C., Affleck, A., and Halliday, G.M. (2013). Classification of FTLD-TDP cases into pathological subtypes using antibodies against phosphorylated and non-phosphorylated TDP43. Acta Neuropathol. Commun. *1*, 33.

Tan, R.H., Ke, Y.D., Ittner, L.M., and Halliday, G.M. (2017). ALS/FTLD: experimental models and reality. Acta Neuropathol. (Berl.) *133*, 177–196.

Tschenett, A., Singewald, N., Carli, M., Balducci, C., Salchner, P., Vezzani, A., Herzog, H., and Sperk, G. (2003). Reduced anxiety and improved stress coping ability in mice lacking NPY-Y2 receptors. Eur. J. Neurosci. *18*, 143–148.

Vernay, A., Sellal, F., and René, F. (2016). Evaluating Behavior in Mouse Models of the Behavioral Variant of Frontotemporal Dementia: Which Test for Which Symptom? Neurodegener. Dis. *16*, 127–139.

Wood, E.M., Falcone, D., Suh, E., Irwin, D.J., Chen-Plotkin, A.S., Lee, E.B., Xie, S.X., Van Deerlin, V.M., and Grossman, M. (2013). Development and Validation of Pedigree Classification Criteria for Frontotemporal Lobar Degeneration. JAMA Neurol. *70*, 1411.

Wu, L.-S., Cheng, W.-C., and Shen, C.-K.J. (2012). Targeted depletion of TDP-43 expression in the spinal cord motor neurons leads to the development of amyotrophic lateral sclerosis-like phenotypes in mice. J. Biol. Chem. *287*, 27335–27344.

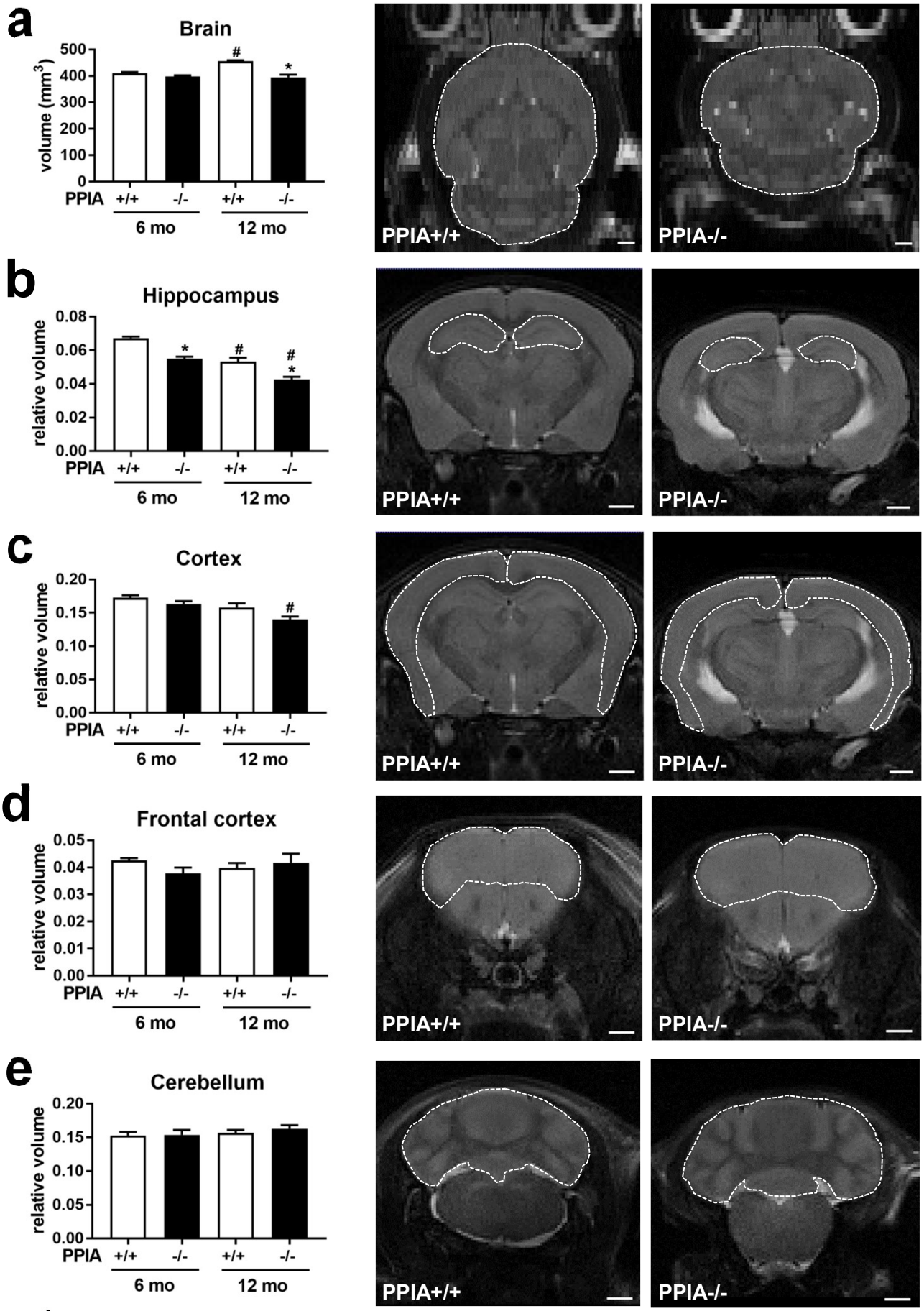

Figure 1

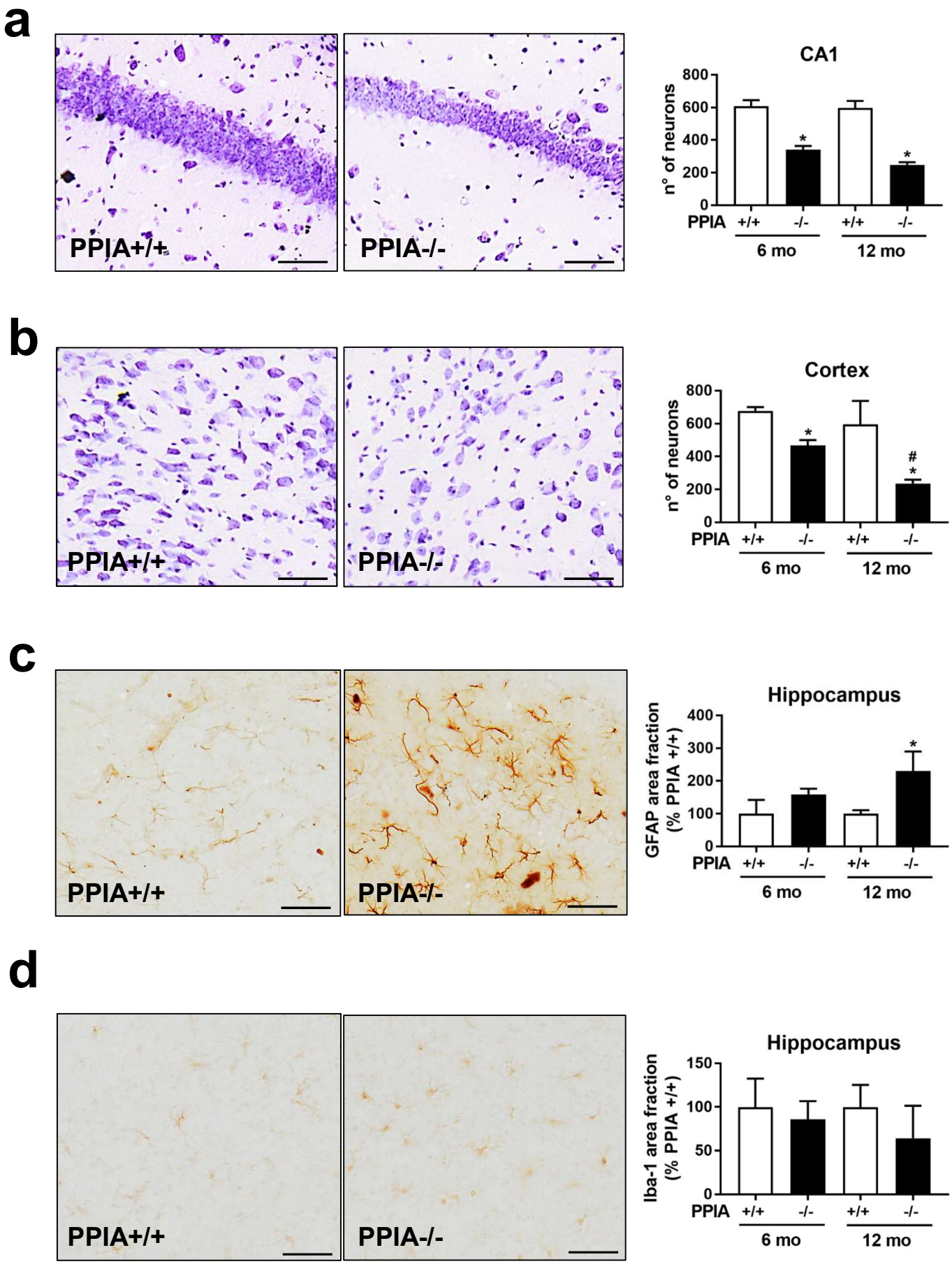

Figure 2

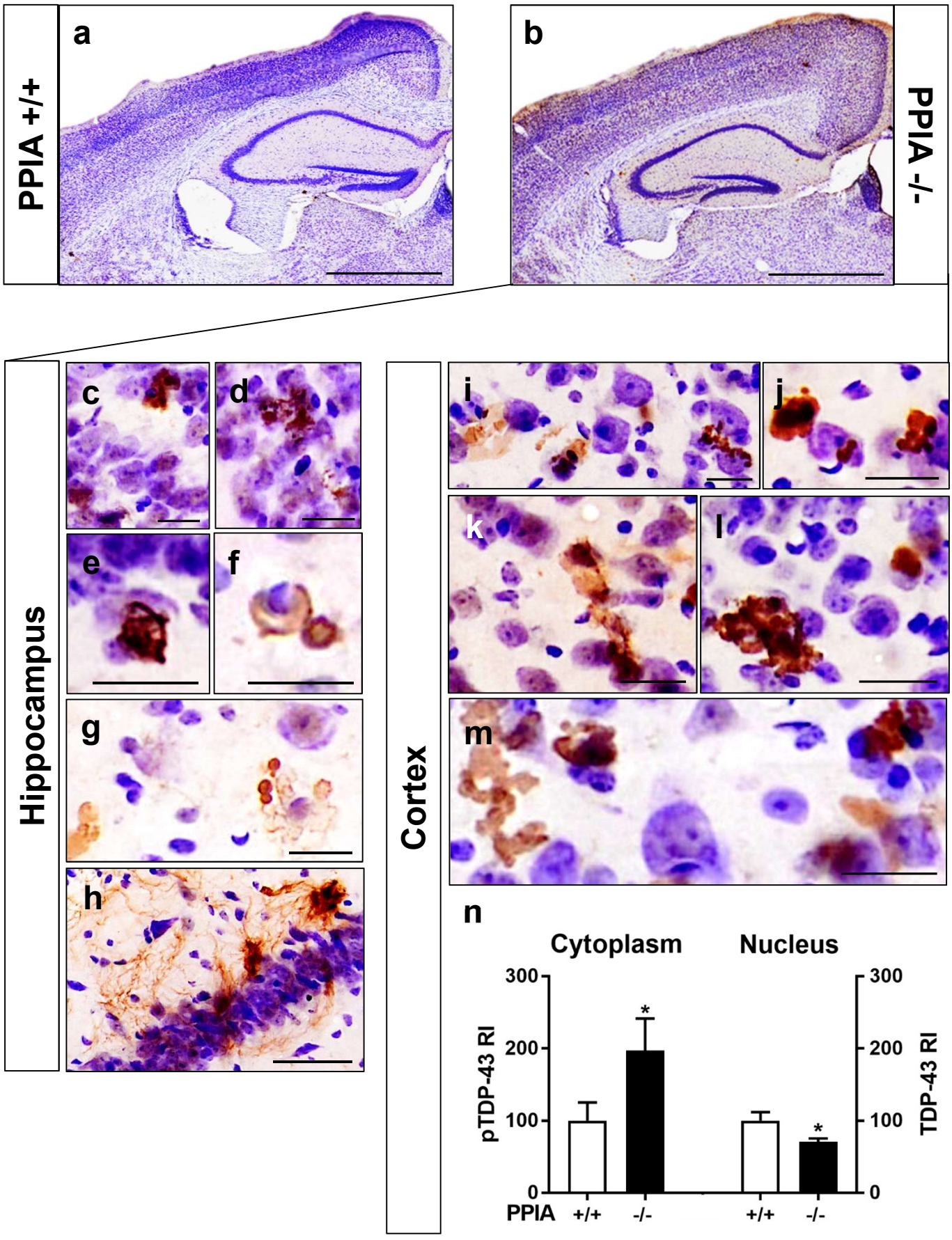

Figure 3

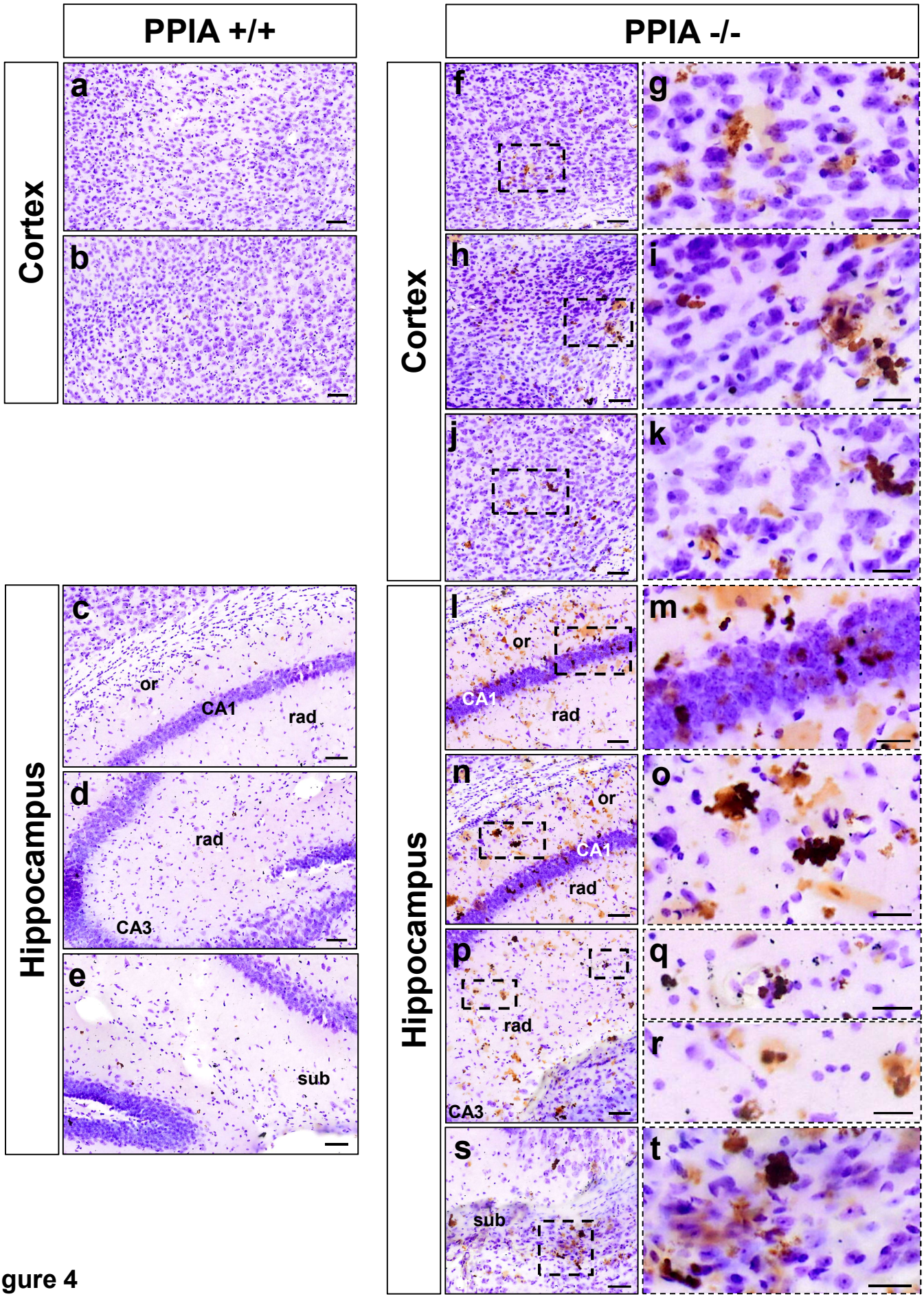

Figure 4

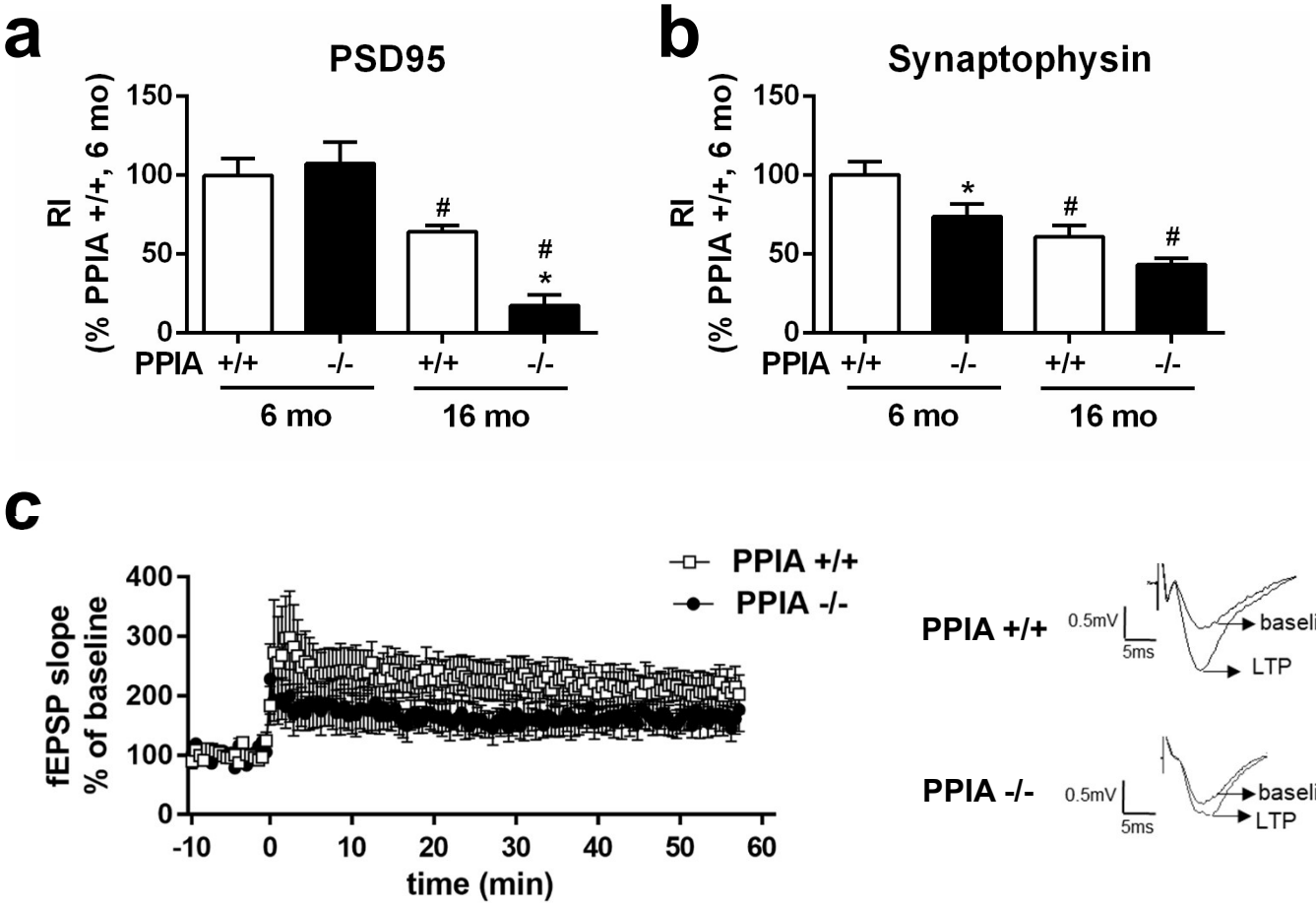

Figure 5

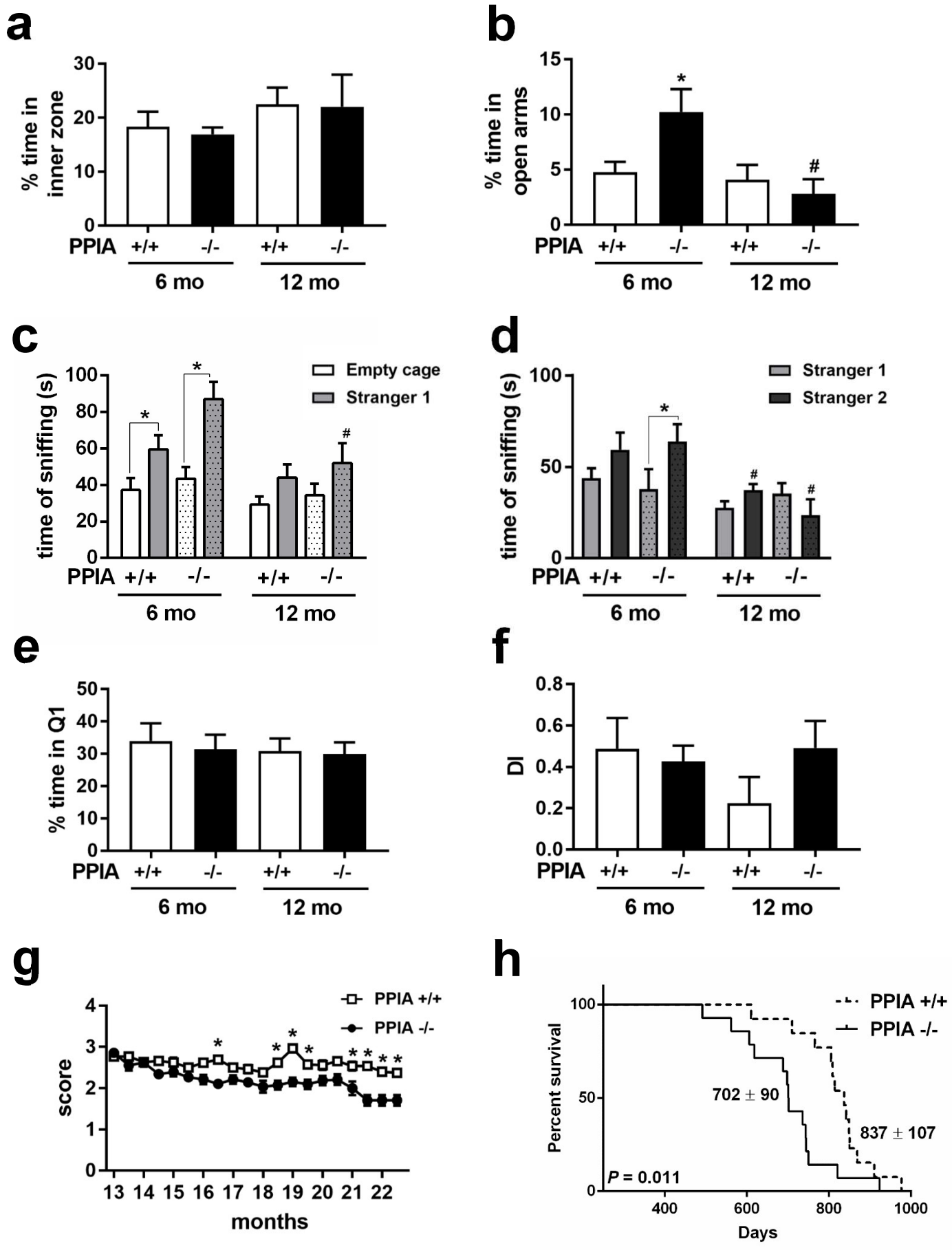

Figure 6

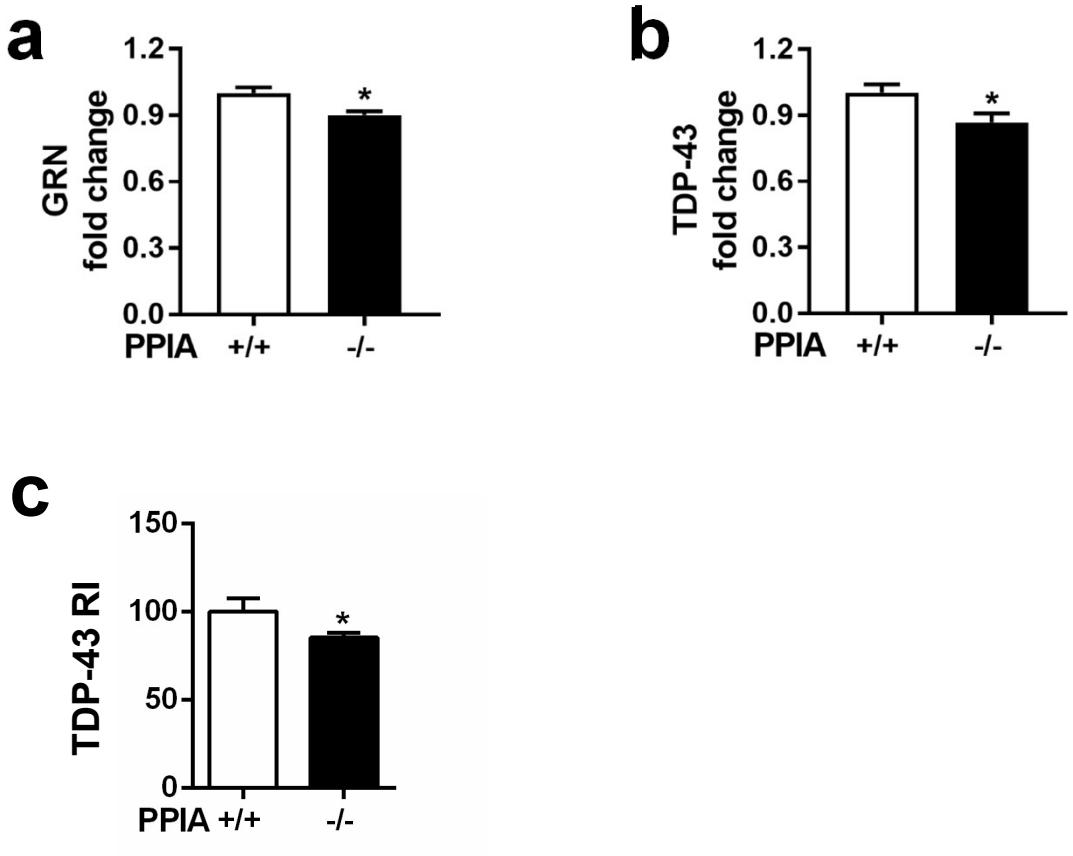

Figure 7

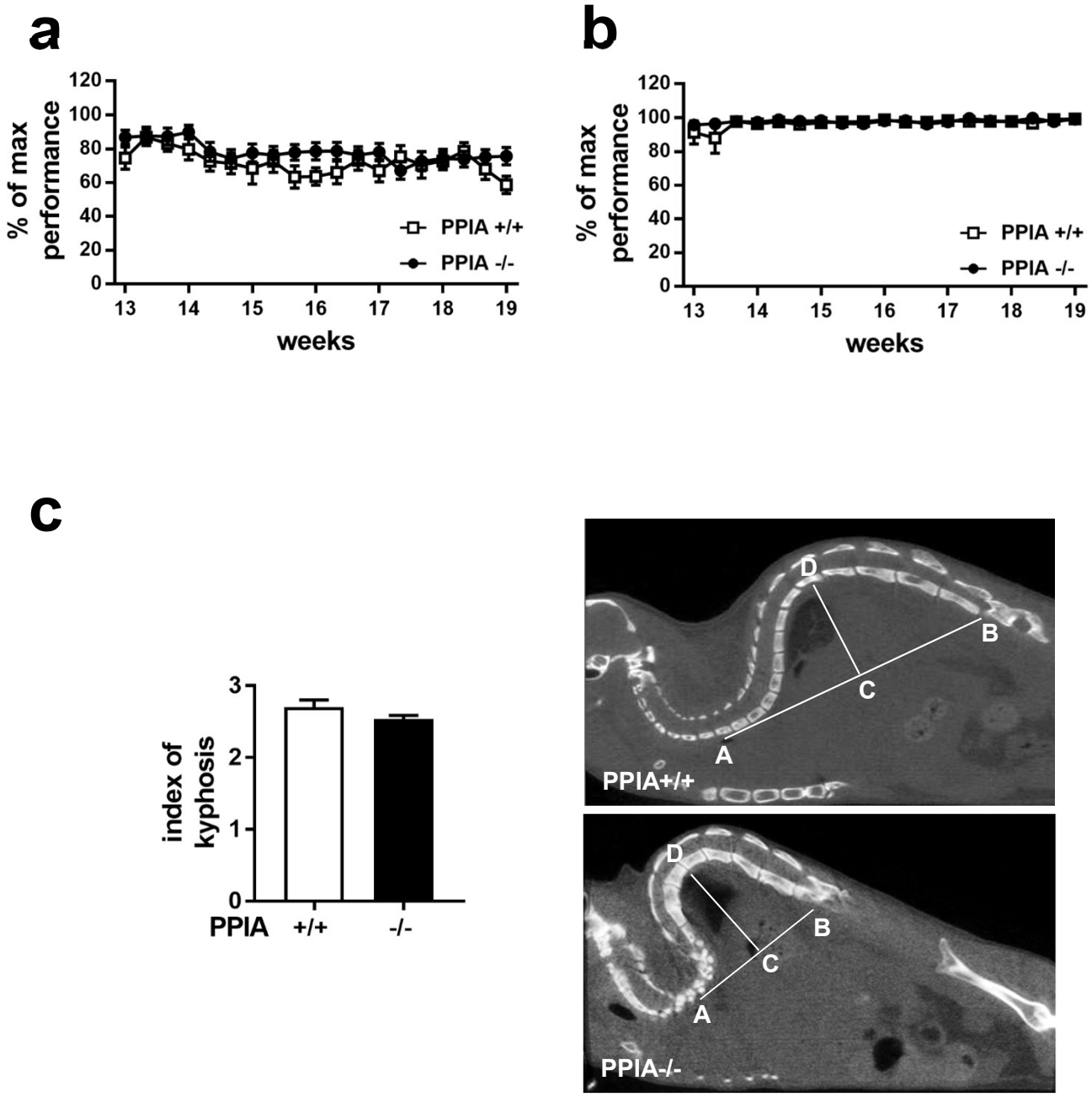

Supplementary Figure 1

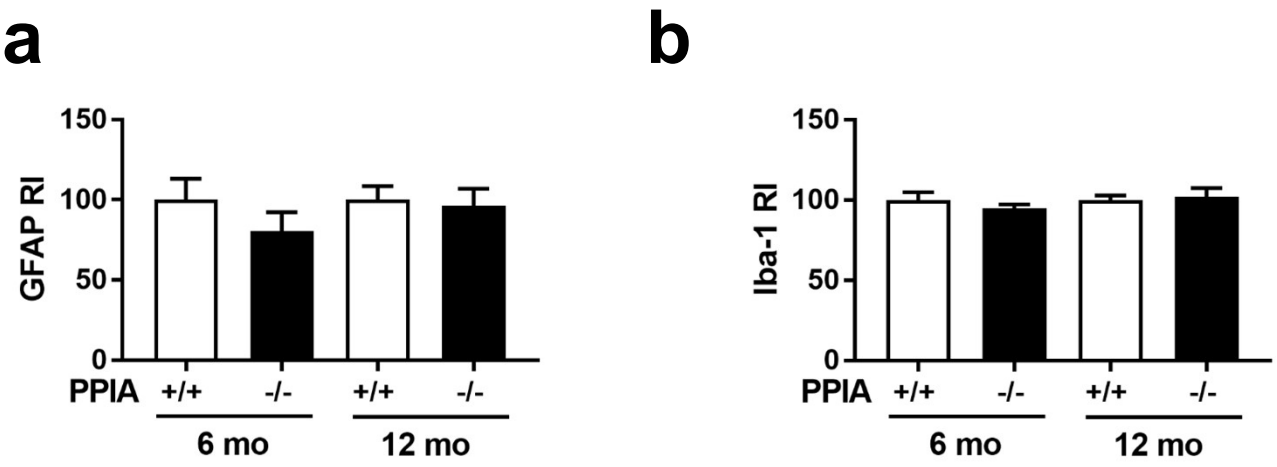

Supplementary Figure 2

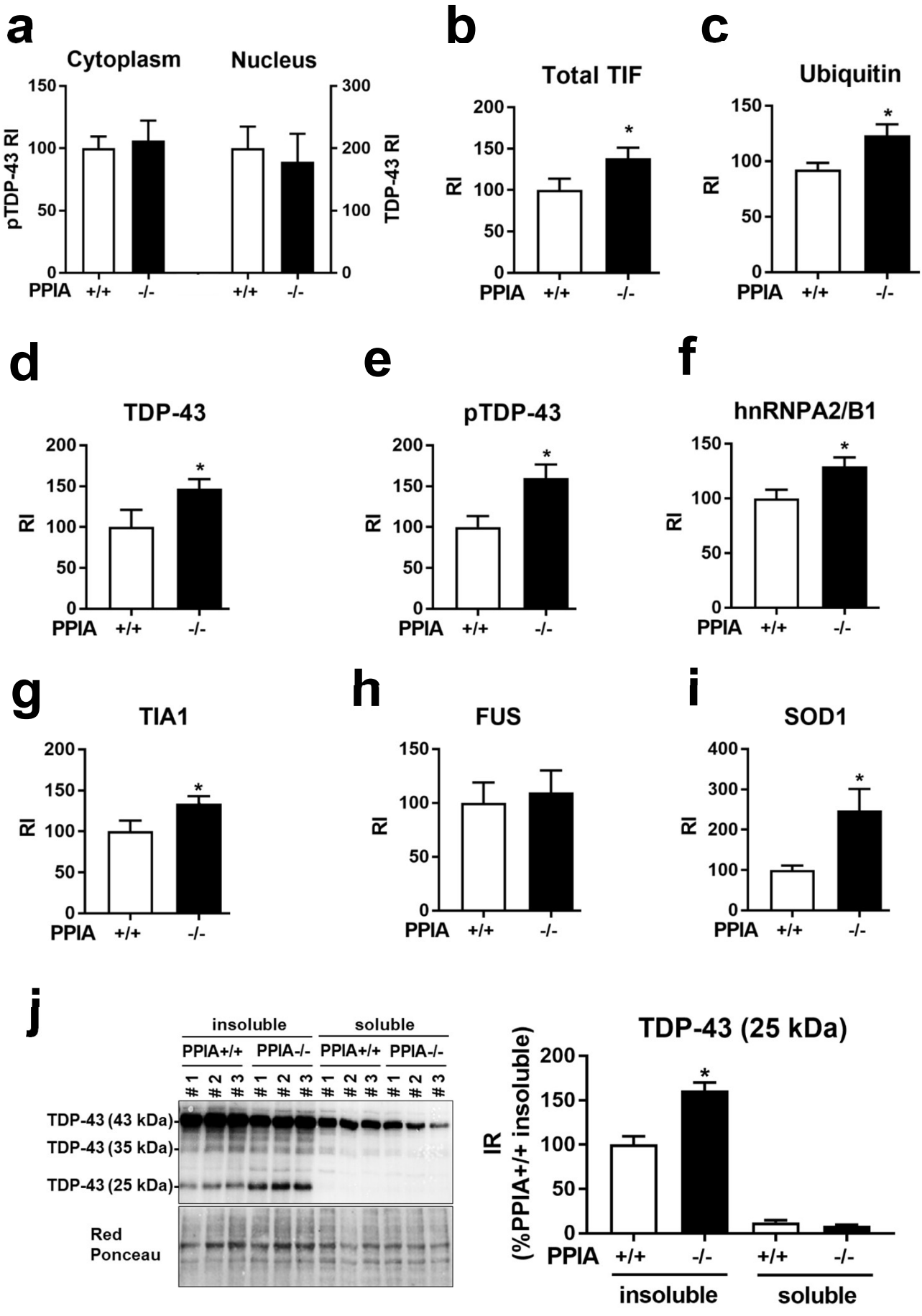

Supplementary Figure 3

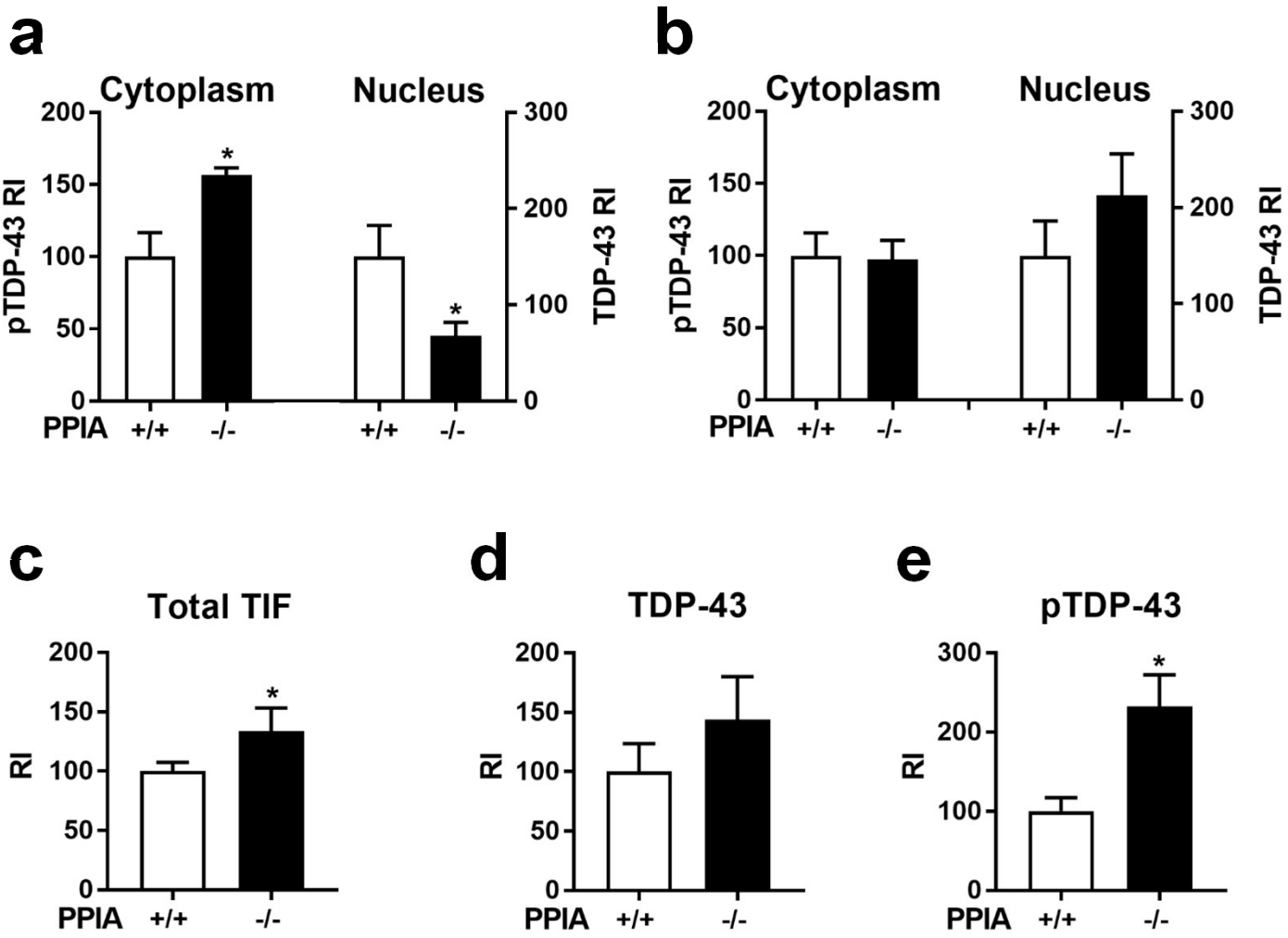

Supplementary Figure 4

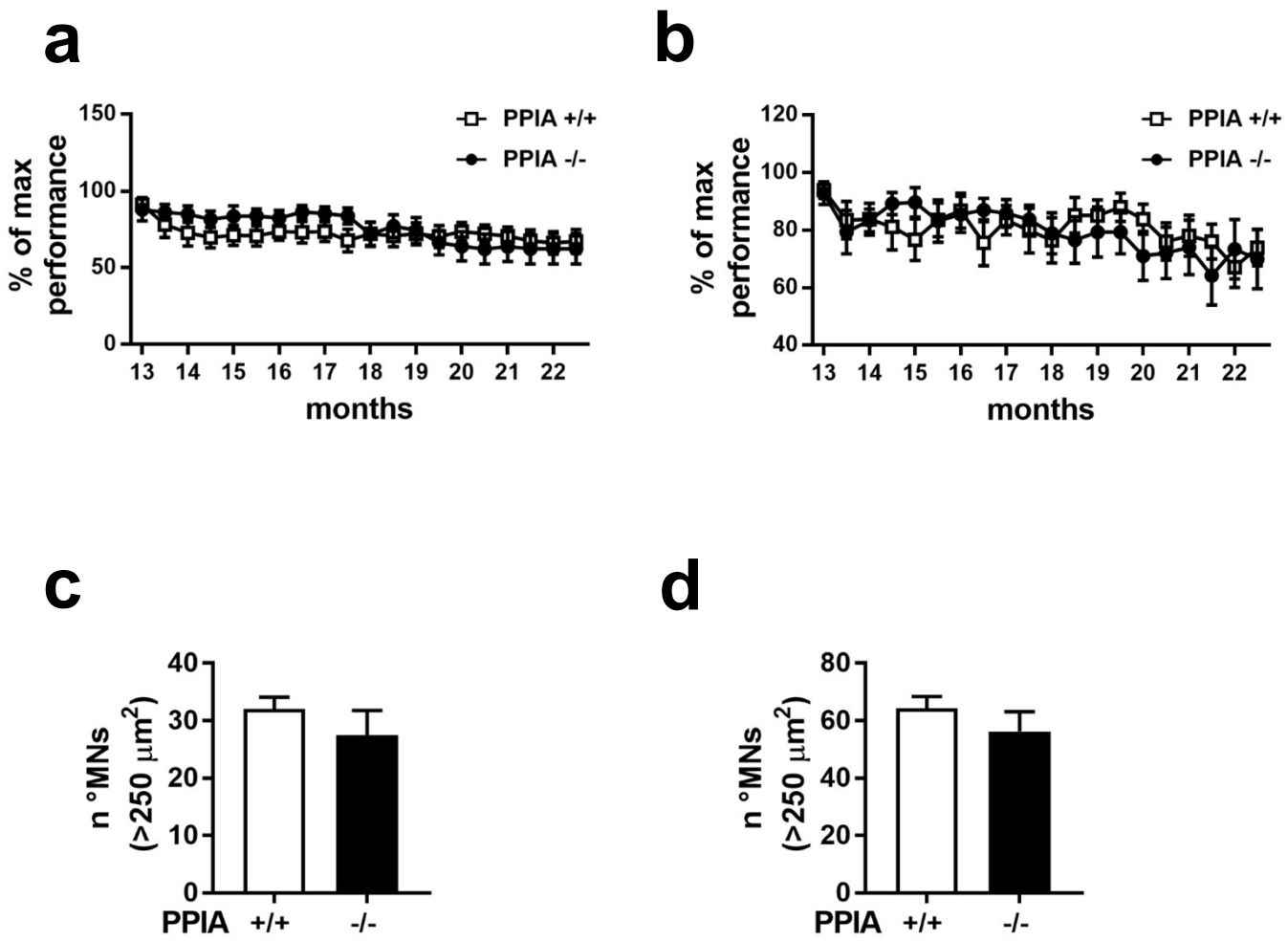

Supplementary Figure 5